

Contrasting origin of post-collisional high-K calc-alkaline and shoshonitic versus alkaline and peralkaline granitoids. The use of sliding normalization

Jean-Paul Liégeois ^{a,*}, Jacques Navez ^a, Jan Hertogen ^b, Russell Black ^c

^a *Département de Géologie, Musée Royal de l'Afrique Centrale, B-3080 Tervuren, Belgium*

^b *Fysico-chemische Geologie, Universiteit Leuven, Celestijnenlaan 200C, B-3001 Heverlee, Belgium*

^c *CNRS ESA7058, Laboratoire de Minéralogie, Muséum National d'Histoire Naturelle, 61 rue Buffon, F-75005 Paris, France*

Received 5 February 1998; accepted 17 June 1998

Abstract

Abundant high-K calc-alkaline (HKCA) magmatism appears to be post-collisional and often shifts to shoshonitic or alkaline–peralkaline compositions in the final stages of orogeny. The nature and the causes of this transition are studied on the basis of 308 major element and of 86 unpublished trace element (including REE) analyses of the Pan-African granitoids from the Tuareg shield (Adrar des Iforas, Mali and Air, Niger). This database covers a wide variety of magmas from subduction-related to intraplate-type including abundant HKCA batholiths. Literature data from geodynamically well-constrained cases are also included. In addition to a conventional geochemical approach of the studied magmatism, the sliding normalization method is proposed. This tool aims at comparing magmatic series: each studied rock is normalized to the interpolated composition of the reference series that has the same SiO₂ content as the sample. This method amplifies differences in sources and in fractionation processes and allows comparison of rocks from basic to acid composition. Two distinct juvenile sources are proposed: a previously enriched phlogopite-K richterite bearing lithospheric mantle or a lower juvenile crustal equivalent for HKCA-shoshonitic magmas, and a lowest lithospheric-upper asthenospheric OIB-type mantle for alkaline-peralkaline magmatism. The first source is melted only shortly after its generation when the lithosphere was still hot, which restricts HKCA magmatism mainly to post-collisional settings. The second asthenospheric/lowest lithosphere source is by definition close to its melting temperature and can generate magma ubiquitously both in space and time. The main melting triggers are lithospheric major structures which are not only operative in a post-collisional setting but also in other environments such as intraplate setting. Geochemistry thus gives indications about the nature of the source and on geotectonic settings. However, the latter is a second rank information, which is partly model-dependant. The post-collisional period differs from other settings by a propensity to generate large amounts of magma of various kinds, among which HKCA magmatism is volumetrically the most prominent. © 1998 Elsevier Science B.V. All rights reserved.

Keywords: High-K calc-alkaline; Alkaline; Geochemistry; Sliding normalization; Granite; Tuareg shield

* Corresponding author. Tel.: 32-2-6502252/42; Fax: +32-2-650-2226; E-mail: jplieg@ulb.ac.be

1. Introduction

After a collision, marked by intense high-pressure regional metamorphism, important amounts of high-K calc-alkaline granitoids are often emplaced, mainly as batholiths. This post-collisional plutonism either dies out with minor amounts of evolved high-K calc-alkaline high-level plutons or is replaced by alkaline magmatism, often as ring complexes, both marking the end of the orogeny (Liégeois et al., 1987, 1994; Sylvester, 1989; Bonin, 1990).

Since 35–40% of granitoids have high-K calc-alkaline compositions (Roberts and Clemens, 1993), it is of high relevance to better define their origin and conditions of generation. The common link with

subsequent alkaline magmatism has also to be understood as a normal evolution of a calc-alkaline source or as a succession of sources. In particular, evolved high-K calc-alkaline and shoshonitic granitoids generally fall within the geochemical fields defined for A-type granitoids, a convergence that has to be decrypted. Conventional geochemical discrimination diagrams are indeed not highly informative in the case of post-collisional granitoids (Pearce, 1996). Moreover, there is a need for a precise definition of alkaline granitoid (vs. peralkaline) or of alkaline series.

These questions constitute the aim of this study, taking the Tuareg shield, NW Africa, as a reference and applying the concepts found to case studies

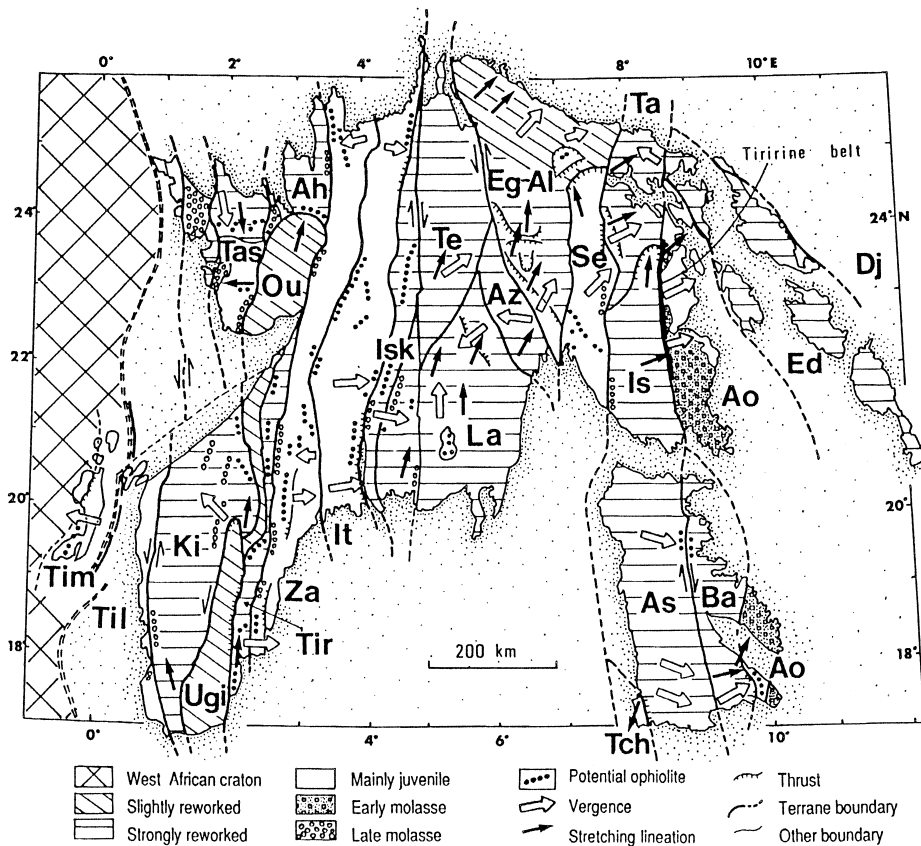


Fig. 1. Tuareg shield terrane map (from Black et al., 1994). Solid arrow = movement direction. Double dashed line is the eastern boundary of the West African craton as marked by gravity anomalies. From east to west, 23 terranes are Djanet (Dj), Edembo (Ed), Aouzegueur (Ao), Barghot (Ba), Assodé-Issalane (As-Is), Tchilit (Tch), Tazat (Ta), Sérouénout (Se), Egéré-Aleksod (Eg-Al), Azrou-n-Fad (Az), Tefedest (Te), Laouni (La), Iskel (Isk), In Teidini (It), Tin Zaouatene (Za), Tirek (Tir), Ahnet (Ah), In Ouzzal (Ou), Iforas granulitic unit (Ugi), Tassendjanet (Tas), Kidal (Ki), Tilemsi (Til), Timétrine (Tim).

elsewhere in the world. The Tuareg shield (500 000 km²), built during the Pan-African orogeny (750–550 Ma), consists for 40% of post-collisional granitoids, most of them being high-K calc-alkaline (Black et al., 1994; Fig. 1). Moreover, it shows a transition to a voluminous post-collisional alkaline magmatism in the Adrar des Iforas (SW Tuareg shield; Liégeois and Black, 1987) while anorogenic alkaline magmatism repeatedly occurred principally during the Devonian in the Aïr massif (Moreau et al., 1994) and during the Quaternary in Central Hoggar and Aïr (Black and Girod, 1970).

2. Salient features of the Tuareg shield

Post-collisional magmatism is variably distributed among the 23 terranes of the Tuareg shield (Black et al., 1994; Fig. 1). It is linked to the relative movements of the terranes along mega-shear zones and occasionally to mega-basal thrusts (Liégeois et al., 1994).

The main collision took place at ~ 750 Ma between the eastern Tuareg terranes (Eastern Hoggar in Algeria and Aïr in Niger) and the East Saharan craton (ESC). Two terranes (Barghot, Aouzegueur) were thrust upon the ESC with concomitant emplacement of calc-alkaline batholiths and plutons (720–665 Ma). Other terranes, like Assodé, collided with the ESC, inducing a phase of regional partial melting of the lower crust which ended there at 666 Ma (Liégeois et al., 1994). Ultimately, this intense collision gave rise to lithospheric delamination of the ESC, on the base of which Black and Liégeois (1993) introduced the notion of an 'East Saharan ghost craton'.

Late Pan-African events (650–550 Ma) are mainly marked by a general northward migration of the Tuareg terranes along N–S mega-shear zones accompanied by high temperature regional metamorphism and the intrusion of abundant high-K calc-alkaline batholiths. This orogenic phase ended with the emplacement of high-level high-K calc-alkaline plutons with alkaline affinities, very rare shoshonitic rocks, and of spectacular alkaline and peralkaline dyke swarms, plateau lavas and ring complexes to the west of the shield (Ba et al., 1985; Liégeois and Black, 1987; Hadj Kaddour et al., 1998). This sec-

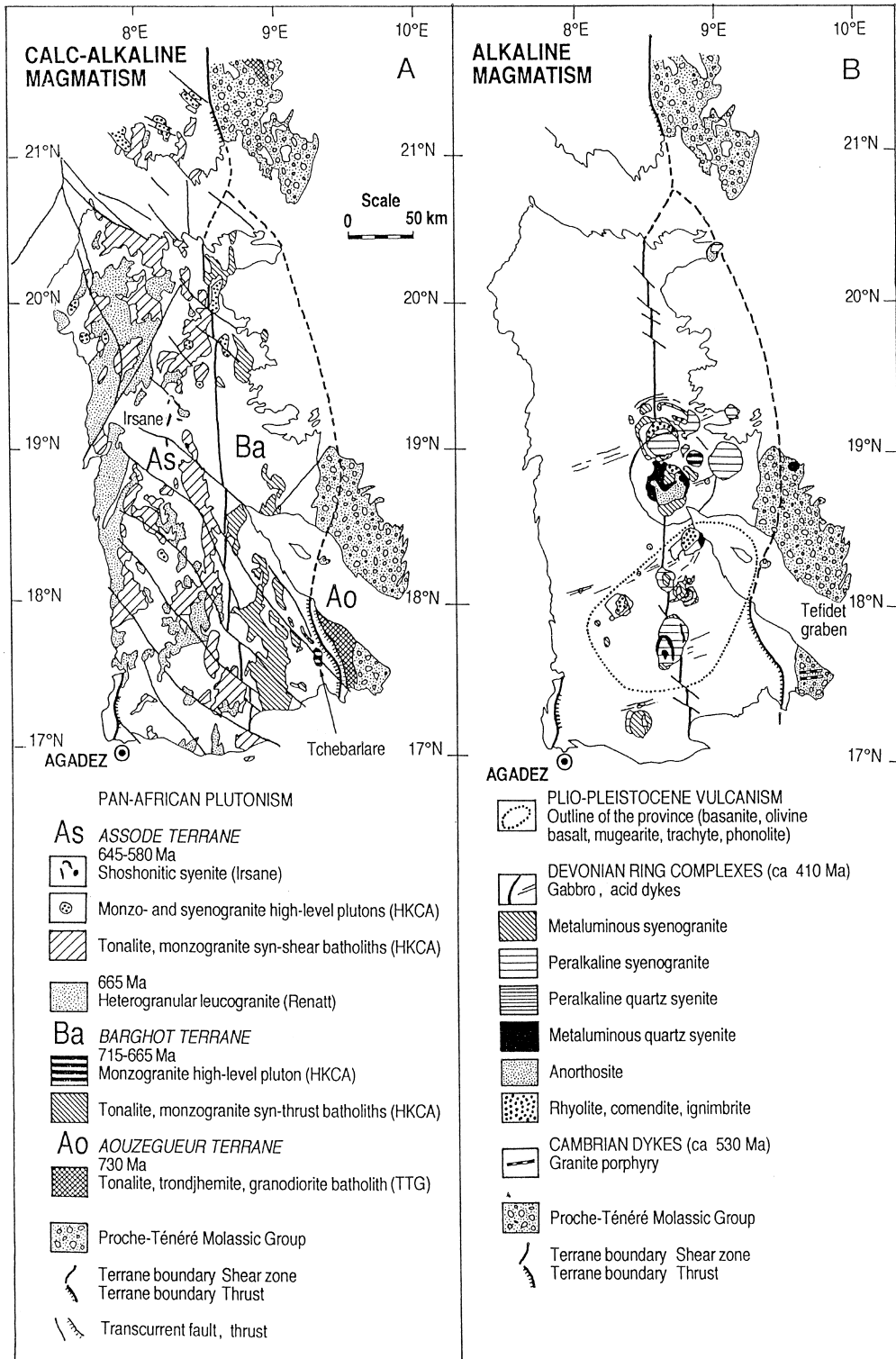
ond Pan-African orogenic phase is mainly driven by the oblique collision of the shield with the West African craton (WAC), which began at 630–620 Ma (Caby et al., 1989) and was largely completed at 580 Ma when most movements along the shear zones stopped (Liégeois et al., 1987, 1994). However, some jolts took place as late as 540 Ma (Boullier et al., 1986) and 525 Ma (Paquette et al., 1998), and were marked by brittle tectonics and emplacement of high-level plutons (Azzouni-Sekkal and Boissonnas, 1993). The docking character of this collision between the Tuareg shield and the WAC allowed the preservation of pre-collisional structures or lithologies. An example is the Tilemsi 730–720 Ma old oceanic island arc (Caby et al., 1989), which is nonetheless located just to the east of the suture with the WAC (Fig. 1). Most of the energy of the collision has been probably absorbed more to the south by the Nigeria-Benin shield, which collided with a WAC indenter (Liégeois et al., 1987).

This long post-collisional period, relative to the early collision with the ESC at 750 Ma, is marked by relative movements of terranes already more or less amalgamated, as evidence for a metamorphic phase at ca. 750 Ma has been found in several of them. These movements were probably driven by one or several subductions located to the west, that have brought the WAC against the Tuareg shield. Hence, these subductions had repercussions on terranes already transformed by a previous subduction period followed by collision that had modified the composition and rheology of the crust and the lithospheric mantle. This geological context was obviously favourable for the generation of high-K calc-alkaline and alkaline magma, given the large volume of magma produced.

This shows also the intertwining of the notions of subduction, collision and post-collision if a sufficiently large area is considered. Even the true anorogenic intraplate magmatism can be often considered as linked to collision occurring at plate edges (Black et al., 1985).

3. The Tuareg shield post-collisional magmatism

Two areas have been selected for this study: the Aïr massif (Niger, SE Tuareg shield; Fig. 2) and the



Adrar des Iforas (Mali, SW Tuareg shield; Fig. 3). They are both relatively well known (Black et al., 1979; Caby et al., 1981; Liégeois et al., 1994), and they comprise moreover the whole gamut of post-collisional Tuareg magmatic types. Air has preserved early active margin-related phases, and the Adrar des Iforas has been the locus of abundant late alkaline magmatism. Both regions comprise abundant high-K calc-alkaline batholiths. These granitoids can be grouped into the following series.

3.1. *Syn-thrust high-K calc-alkaline granitoids*

They lie within the Barghot terrane in Air (Fig. 2A). The collision with the ESC at ca. 750 Ma (Boven et al., in prep.) induced a regional metamorphism in the amphibolite facies (peak at 680°C and 8 kbar; Liégeois et al., 1994). The Barghot terrane has been rapidly thrust upon the ESC during which sills of high-K calc-alkaline (HKCA) granitoids intruded. They are intercalated within the gneissic foliation except for some rare late high-level plutons that truncate the thrust structure (e.g., Tchebarlare pluton, Fig. 2A). They contain abundant mafic enclaves showing mixing/mingling features. Their syn-thrust emplacement stretched from 720–700 to 665 Ma for the late phases (Liégeois et al., 1994). These granitoids have been classified as post-collisional because they post-date the metamorphic climax (ca. 750 Ma). However they could be also considered as syn-collisional. To avoid any ambiguity, they will be referred to as ‘syn-thrust HKCA’.

3.2. *Syn-shear high-K calc-alkaline granitoids*

The members of this group studied in this paper form large NS-elongated batholiths in the Assodé terrane from the Air massif (Figs. 1 and 2A) and in the Kidal terrane from the Adrar des Iforas (Figs. 1 and 3A). In volume, this is clearly the most important group.

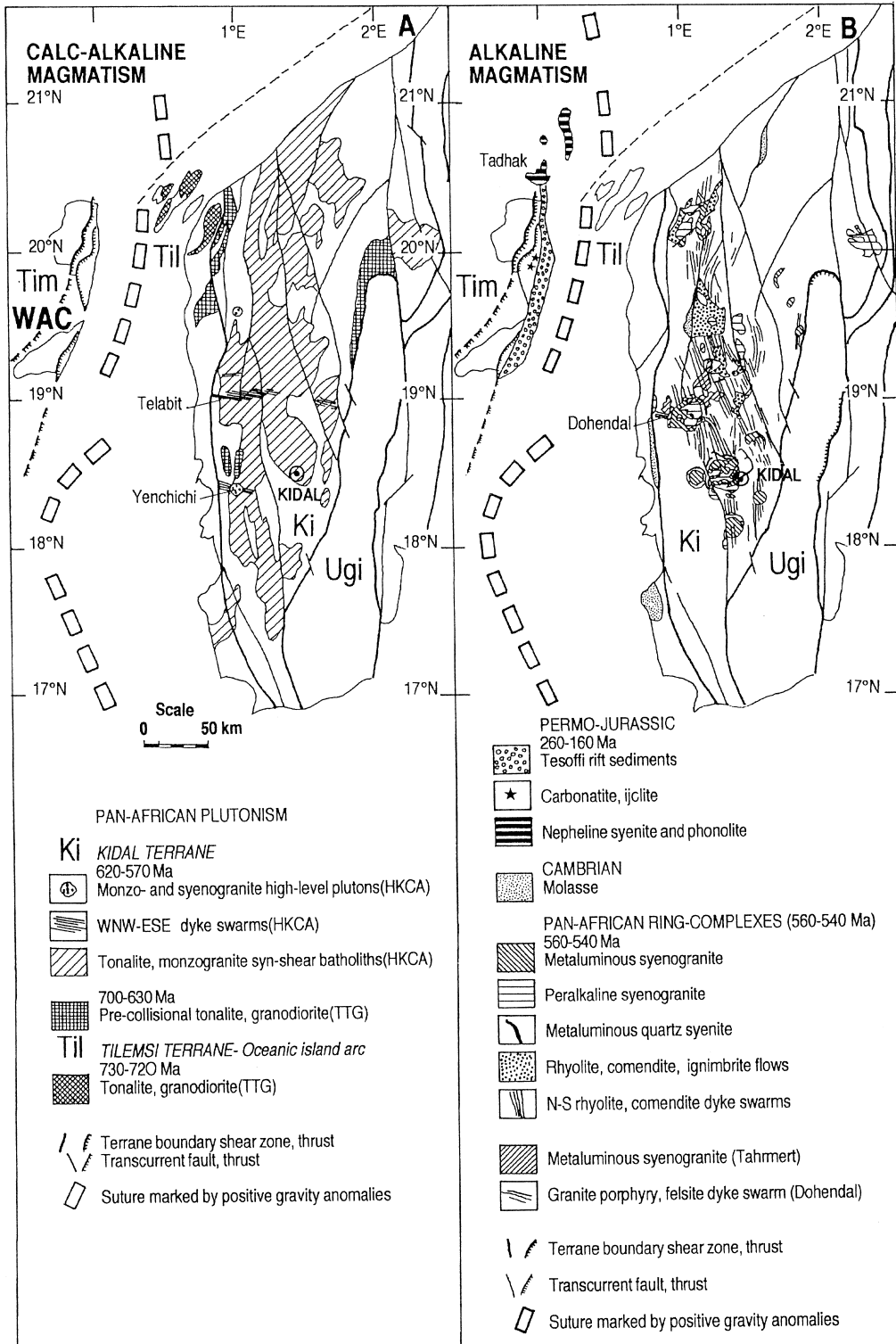
After collision with the ESC, the Assodé terrane has been invaded by a widespread potassic leucogranite (Renatt syenogranite) dated at 666 ± 11

Ma. Liégeois et al. (1994) suggested that this granite formed by partial melting of the felsic lower crust in response to a rapid upwelling of the asthenosphere due to a lithospheric delamination. This thin lithospheric mantle moreover favoured the sliding of this terrane to the north along the ESC western margin (Raghane mega-shear zone; Fig. 2). It is inferred that this movement occurred on 1000 km over a period of 65 Ma at 645–580 Ma, during which batholiths were emplaced. These batholiths as well as the subsequent high-level circular plutons are high-K calc-alkaline in nature.

Early Pan-African events have been recognized in the Kidal terrane (Caby and Andreopoulos-Renaud, 1985) but have been poorly studied. Granitoids from this phase are unconformably overlain by volcano-sedimentary sequences that mark the beginning of the late Pan-African docking. Most of the geological events in the Kidal terrane occurred over the 635–540 Ma time span, during which the huge Iforas batholith intruded (Liégeois and Black, 1987; Liégeois, 1988; Fig. 3A), also elongated along the N-S mega-shear zones delimiting the Kidal terrane. Main high-K calc-alkaline intrusions occurred between 620 and 580 Ma. Late intrusions of similar chemistry are represented by E–W oriented dyke swarms and less voluminous high-level circular plutons (Fig. 3A). As the syn-thrust group, these granitoids often contain microgranular mafic enclaves, which attest to mixing/mingling features with more mafic magma.

These HKCA batholiths will be called here ‘syn-shear HKCA’, because they intruded during large horizontal movements of terranes after a major collisional impact and represent typical post-collisional magmatism. The huge E–W oriented Telabit dyke swarm (Fig. 3A) and a high-level pluton (Yenchichi 2) are both late manifestations of this group. They have been selected here as the reference series (see below) and will be distinguished as the ‘syn-shear Yenchichi 2-Telabit series’. Shoshonitic magmatism seems to be very rare in the Tuareg shield, as only one homogeneous pluton has been recognized (Irsane pyroxene-amphibole syenite, Fig. 2A). To be able to compare the HKCA and alkaline to shoshonitic mag-

Fig. 2. Air (Niger) geological sketch maps. (A) Calc-alkaline magmatism; (B) Alkaline magmatism (after Black, 1967 and Liégeois et al., 1994).



matism, the Pan-African post-collisional Romanian Tismania pluton (Liégeois et al., 1996a), showing a shoshonitic liquid line of descent from diorite to granite (Duchesne et al., 1998) will be added in the geochemical diagrams.

3.3. Late-shear alkaline-peralkaline acid magmatism

Alkaline rocks are diversely defined in the literature, particularly when they are silica-oversaturated. In the latter case, the classical view is to reserve the term ‘alkaline’ for sodic amphibole- or pyroxene-bearing rocks (Sørensen, 1974). However, this implies that the terms alkaline and peralkaline are synonymous, and that miaskitic metaluminous granitoids closely associated with peralkaline granitoids cannot be considered as alkaline, even when sharing the same origin. To overcome these problems, metaluminous granites occurring within complexes containing peralkaline facies are often considered as alkaline (Black et al., 1985; Bonin, 1986; Liégeois and Black, 1987). These non-peralkaline alkaline granites are generally biotite-bearing alkali feldspar granite or syenogranite, in which K-feldspar always largely predominates on plagioclase. As their petrography is not very different from evolved calc-alkaline granites, they can probably only definitely be ascribed to the alkaline series on geochemical grounds.

Alkaline–peralkaline magmatism is mainly known in the western part of the Tuareg shield in particular in the Adrar des Iforas (Liégeois and Black, 1987). There, it is composed of huge N–S rhyolitic dyke swarms that have fed kilometer-thick rhyolitic plateaux and of 15 ring complexes, some of which attain a diameter of 25–30 km (Ba et al., 1985). These ring complexes show no spatial age trend (Liégeois et al., 1996b). Early alkaline manifestations (Fig. 3B) exhibit a hybrid character, both in their mineralogy and chemistry (Ba et al., 1985; Liégeois and Black, 1987). The emplacement of this alkaline province is linked to post-collisional stress reversals along shear zones (Boullier et al., 1986) and occurred between 560 and 540 Ma (Liégeois et

al., 1987, 1996b). It will be called here the ‘late-shear alkaline’ group.

The gigantic volume of this post-collisional alkaline magmatism (Fig. 3B) stands out clearly against the minor amounts which characterize the waning stages of the calc-alkaline magmatism in both the Assodé and Kidal terranes and elsewhere in the Tuareg shield. The Air massif comprises also large alkaline anorthosite-bearing ring-complexes (Fig. 2B) but they are clearly anorogenic (ca. 410 Ma; Moreau et al., 1994) and dyke swarms are rare.

3.4. An additional reference series: the pre-collisional calc-alkaline magmatism

Due to the slight intensity of the docking at ca. 600 Ma between the WAC and the Tuareg shield, pre-collisional lithologies have been preserved to the west as the Tilemsi 730–700 Ma old oceanic arc (Caby et al., 1989) or as ca. 700–630 Ma granodiorites and tonalites in the Kidal terrane (Bertrand et al., 1984; Caby and Andreopoulos-Renaud, 1985; Liégeois et al., 1987). On the other side of the Tuareg shield, a tonalite-trondjemite-granodiorite (TTG) series has been preserved in the Aouzegueur terrane (Fig. 1), due to its early thrusting upon the ESC (Liégeois et al., 1994). These granitoids are mainly medium-K calc-alkaline and will be called ‘pre-collisional TTG’ group.

4. Isotopic signature of the different groups

Isotopic data for Nd and Sr can be found in Black et al. (1991) and Liégeois et al. (1994) for the Air, in Caby et al. (1989) for the Tilemsi island arc, and in Liégeois and Black (1984, 1987) and Liégeois (1988) for the Kidal terrane in the Adrar des Iforas. A summary is given in Table 1 for ready access.

Mantle and crustal reservoirs have been measured in the Tuareg shield through local representative lithologies. Depleted mantle values have been obtained on the Tilemsi oceanic island arc in the Adrar des Iforas (Fig. 1) giving, at 730 Ma, $Sr_1 = 0.7024$

Fig. 3. Adrar des Iforas (Mali) geological sketch maps. (A) Calc-alkaline magmatism; (B) Alkaline magmatism (after Fabre, 1982). The scale is the same as in Fig. 2.

Table 1
Summary of Sr and Nd initial ratios from Adrar des Iforas and Aïr

| Group | Terrane | Pluton | Age | Sample | Sr _i | Sr _i isochrone | ε _{Nd} | Ref. | |
|----------------------------|------------|-------------|-----------|-----------|---------------------|--|---------------------|---------|--------------------|
| Pre-collision TTG | Aouzegueur | Eberjegui | 730 Ma | BLN6 | 0.70560 | 0.70358 ± 21 (8 WR) | −9.8 | 1 | |
| | | | | BLN15 | 0.70702 | | −12.7 | | |
| | | | | BLN16 | 0.70476 | | −7.0 | | |
| | Kidal | Erecher | 630 Ma | JPL280 | 0.70531 | | −11.8 | 2, 3 | |
| | | | | JPL286 | 0.70580 | | −12.0 | | |
| | | | | JPL290 | 0.70582 | | −12.5 | | |
| Syn-thrust HKCA | Barghot | Beurhot | 700 Ma | V67 | 0.70392 | 0.70884 ± 36 (7 WR) | −8.5 | 1 | |
| | | | | V72 | 0.70373 | | −0.6 | | |
| | | | | V73 | 0.70311 | | −2.5 | | |
| | Barghot | Takarakoum | 700 Ma | BLN57 | 0.70897 | | −10.2 | 1 | |
| | | | | BLN58 | 0.70924 | | −10.8 | | |
| | | | | BLN60 | 0.70897 | | −10.2 | | |
| | Barghot | Tchebarlare | 664 Ma | BLN34 | 0.70527 | | −8.2 | 4 | |
| | | | | BLN38 | 0.70493 | | −8.5 | | |
| | | | | BLN38 | 0.70493 | | −2.5 | | |
| | Assodé | Ifrouâne | 600 Ma | BLN103 | 0.70944 | | 0.70957 ± 34 (7 WR) | −14.7 | 4 |
| | | | | BLN104 | 0.71017 | | | −13.0 | |
| | | | | BLN110 | 0.71110 | | | −12.6 | |
| BLN112 | | | | 0.71092 | −14.9 | | | | |
| Assodé | Teggar | 600 Ma | BLN131 | 0.71455 | 0.7183 ± 144 (6 WR) | −17.4 | 4 | | |
| | | | BLN139 | 0.71148 | | −7.9 | | | |
| Syn-shear HKCA | Kidal | Adma | 595 Ma | JPL238 | 0.70483 | 0.70482 ± 26 (9WR) | −6.2 | 2, 3 | |
| | | | | JPL243 | 0.70488 | | −6.4 | | |
| Late-shear ALK | Kidal | Aoukenek | 590 Ma | JPL369 | 0.70335 | 0.7035 ± 5 (7 WR) | −0.7 | 2, 3 | |
| | | | | N–S dykes | 545 Ma | | JPL375 | | 0.70356 |
| | | JPL376 | 0.70397 | | | | −2.8 | | |
| | | JPL403 | 0.70466 | | | | −5.2 | | |
| | | Kidal | 560 Ma | | | | B20 | 0.70726 | 0.7061 ± 7 (25 WR) |
| | | | | RB455 | 0.70538 | | −0.9 | | |
| JPL234 | 0.70317 | −1.9 | | | | | | | |
| Regional anatectic granite | Assodé | Renatt | 666 Ma | BLN144 | 0.70970 | 0.7121 ± 4 (9 WR) (for lower crustal melts; see text) | −22.7 | 4 | |
| | | | | BLN145 | 0.74173 | | −22.9 | | |
| | | | | BLN150 | 0.76751 | | −13.6 | | |
| | | | | BLN308 | 0.71501 | | −22.5 | | |
| | | | | BLN321 | 0.74508 | | −16.2 | | |
| Archaean lower crust UGI | UGI | | at 600 Ma | JPL485 | 0.71699 | | −23.7 | 3 | |
| | | | | JPL486 | 0.71465 | | −23.7 | | |
| | | | | JPL487 | 0.70742 | | −23.2 | | |
| | | | | JPL487 | 0.70742 | | −23.2 | | |

References: (1) Black et al., 1991; (2) Liégeois and Black, 1984; (3) Liégeois, 1988; (4) Liégeois et al., 1994.

and $\epsilon_{Nd} = +6.5$ (Caby et al., 1989). Old lower continental crust isotopic characteristics have been calculated for 700–600 Ma at $Sr_i = 0.710$ and $\epsilon_{Nd} = -25$ on both the basis of the Archaean granulitic facies gneisses from the UGI terrane in the Adrar des Iforas (Fig. 1; Liégeois, 1988) and on the basis of the Renatt leucogranite in Aïr (Liégeois et al., 1994).

The latter lower crustal melt has strongly interacted with the wet upper crust suggesting values at this period of Sr_i up to 0.780 and ϵ_{Nd} down to -15 for a 2 Ga old upper crust.

When the post-collisional magmatism from the Tuareg shield is plotted together with representative data for crustal and mantle sources (Fig. 4), it

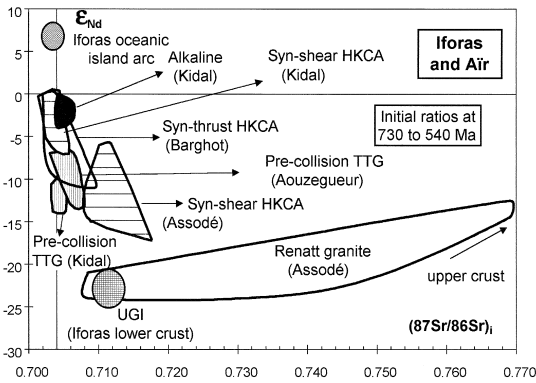


Fig. 4. Sr_i vs. ϵ_{Nd} diagram. Initial ratios have been recalculated to their emplacement age (between 730 and 540 Ma). Data are from Liégeois and Black, 1987; Liégeois, 1988; Caby et al., 1989; Liégeois et al., 1994. See also Table 1.

emerges that all groups record an important interaction between material from a juvenile pole (the mantle or a young crust) and from an old crust, mainly the lower one. The crustal contribution appears to have been more important the Air than in Adrar des Iforas. Crust particularly influenced the syn-shear magmatism from the Assodé terrane, with a more important contribution from the old upper crust than in the other groups (Fig. 4). This has been linked to the preceding regional partial melting of the old crust which affected this terrane, leaving it hot, ductile and then highly reactive (Liégeois et al., 1994). The late members of the different groups are generally closer to the juvenile mantle component of their group. The alkaline group is also relatively close to the juvenile pole. The inverse trend is observed in the Central Bohemian pluton (Janoušek et al., 1995) which suggests that the K enrichment is not linked to the amount of contamination indicated by Sr and Nd isotopes.

Even if the mixing between a juvenile component (either mantle or crust) and an old crustal one seems to be the rule in the post-collisional Tuareg magmatism, the amount of old crustal participation does not seem to substantially influence their bulk chemistry.

5. Geochemical signature of the different groups

New major and trace elements analyses for 86 samples can be found in Table 2. Major element

analyses and Rb, Sr, Zr and Y data for 222 other samples from the Air (Niger) and the Adrar des Iforas (Mali) are available from the first author on request. Analytical techniques are described in Appendix A. Six analyses from the Kidal terrane TTG series have been taken from Bertrand et al. (1984) (samples 1 to 6). The twenty-two analyses of the Tismaña pluton (Romania) are taken from Duchesne et al. (1998). All major elements have been recalculated on an anhydrous basis as recommended by IUGS (Le Maitre, 1989). As considered analyses have all a major oxide sum close to 100% and low water content (Table 2) an alteration bias can be precluded.

Silica and alkalis are at the base of the classification of the granitoids, either petrographical or geochemical (Le Maitre, 1989). The widely used SiO_2 vs. K_2O diagram (Fig. 5A; Rickwood, 1989 and references therein) shows that the major part of the post-collisional magmatism from the Tuareg shield is high-K calc-alkaline (HKCA). The syn-shear Yenchichi 2-Telabit (YT) series defines a regular trend of liquids from 54 to 77% SiO_2 (Liégeois, 1988) which could be called alkali-calcic (Peacock, 1931). It represents the extreme manifestation of the HKCA (non-shoshonitic) group before the appearance of the alkaline group in the Adrar des Iforas. The discrimination diagram for granites ($SiO_2 > 68\%$) based on major elements (Sylvester, 1989; Fig. 5B) indicates that the chosen Tuareg series correspond to standard major element compositions for TTG, calc-alkaline and alkaline series which plot in majority within the expected fields. Some additional observations can be made: (1) numerous samples fall within the common field of alkaline and highly fractionated calc-alkaline rocks although only a poor overlap exists between the two groups within this field; (2) one syn-thrust HKCA pluton (Takarakoum) plots in or very close to the alkaline field; (3) the Tismaña shoshonitic series dissociates from the other series not only by being to the right of the diagram but also by crossing the alkaline boundary. The alkaline magmatism differs from the calc-alkaline series, and particularly from the shoshonitic series, by a higher Na_2O content (Fig. 5C). This is expressed by the presence of sodic Fe–Mg minerals in the peralkaline granites, which are moreover depleted in Al (Table 2; Bonin, 1986). The apgaitic

Table 2
Major and trace elements

| | Pre-collisional TTG (Kt) | | | Pre-collisional TTG (Ao) | | | Takarakoum | | | Beurhot | | | Syn-thrust HKCA (Ba) | | | Tchebatiare | | | Dabagafiférouane | | | Syn-shear HKCA (As) | | | T-nm. | Tamaz. |
|---------------------------------|--------------------------|--------|--------|--------------------------|--------|-------|------------|--------|-------|---------|--------|--------|----------------------|--------|--------|-------------|-------|--------|------------------|--------|--------|---------------------|--------|--|-------|--------|
| | Erecher | JPL289 | JPL286 | JPL293 | JPL280 | BLN16 | BLN15 | BLN17 | BLN57 | BLN68 | BLN70 | V74 | V67 | BLN401 | V36 | BLN34 | V34 | BLN293 | BLN103 | BLN104 | BLN139 | BLN335 | BLN361 | | | |
| SiO ₂ | 70.62 | 70.92 | 69.16 | 72.96 | 76.39 | 59.57 | 60.37 | 68.35 | 68.12 | 59.21 | 69.79 | 71.35 | 72.52 | 69.56 | 68.17 | 71.89 | 75.04 | 70.56 | 70.84 | 73.51 | 75.52 | 72.02 | 75.42 | | | |
| TiO ₂ | 0.46 | 0.39 | 0.36 | 0.25 | 0.16 | 0.70 | 0.77 | 0.26 | 0.41 | 0.92 | 0.42 | 0.25 | 0.40 | 0.37 | 0.40 | 0.27 | 0.07 | 0.38 | 0.36 | 0.17 | 0.11 | 0.42 | 0.24 | | | |
| Al ₂ O ₃ | 14.49 | 14.26 | 13.90 | 13.18 | 12.65 | 16.75 | 16.99 | 17.38 | 15.01 | 17.27 | 15.12 | 15.09 | 14.19 | 15.64 | 14.36 | 13.68 | 13.89 | 14.44 | 14.68 | 13.56 | 13.06 | 14.73 | 12.00 | | | |
| Fe ₂ O ₃ | | | | | | 2.58 | 3.04 | 0.33 | 1.22 | 2.66 | 1.36 | 0.88 | 0.96 | 1.11 | 1.54 | 1.06 | 0.82 | 1.46 | 0.97 | 0.86 | 0.49 | 1.62 | 0.99 | | | |
| FeO | | | | | | 3.45 | 3.17 | 0.81 | 1.52 | 3.18 | 1.72 | 0.63 | 1.21 | 0.95 | 1.22 | 1.63 | 0.95 | 1.24 | 0.84 | 0.92 | 0.41 | 0.69 | 0.85 | | | |
| MnO | 0.10 | 0.10 | 0.08 | 0.06 | 0.05 | 0.10 | 0.12 | 0.06 | 0.04 | 0.30 | 0.07 | 0.03 | 0.04 | 0.05 | 0.06 | 0.03 | 0.01 | 0.05 | 0.03 | 0.04 | 0.03 | 0.05 | 0.05 | | | |
| MgO | 0.92 | 0.76 | 0.90 | 0.54 | 0.26 | 2.72 | 2.75 | 0.51 | 1.00 | 2.30 | 0.89 | 0.37 | 0.71 | 0.70 | 0.78 | 1.97 | 1.00 | 0.78 | 0.41 | 0.40 | 0.13 | 0.47 | 0.24 | | | |
| CaO | 3.15 | 2.89 | 3.25 | 1.78 | 1.02 | 5.58 | 5.58 | 4.44 | 2.86 | 4.81 | 2.67 | 1.38 | 2.03 | 1.43 | 2.50 | 2.01 | 1.05 | 2.14 | 1.43 | 1.44 | 0.94 | 1.79 | 0.94 | | | |
| Na ₂ O | 4.65 | 4.74 | 4.59 | 4.13 | 3.52 | 3.95 | 3.92 | 7.14 | 4.21 | 5.93 | 3.77 | 4.06 | 4.11 | 3.23 | 3.85 | 4.46 | 4.09 | 2.92 | 3.26 | 2.83 | 3.86 | 3.65 | 2.92 | | | |
| K ₂ O | 1.47 | 1.51 | 1.32 | 2.76 | 3.32 | 2.25 | 1.63 | 0.43 | 3.51 | 2.80 | 4.12 | 5.91 | 3.57 | 5.34 | 4.61 | 3.66 | 3.55 | 4.32 | 5.89 | 5.62 | 5.07 | 4.47 | 4.70 | | | |
| P ₂ O ₅ | 0.16 | 0.10 | 0.14 | 0.10 | 0.01 | 0.23 | 0.25 | 0.16 | 0.12 | 0.23 | 0.11 | 0.07 | 0.14 | 0.10 | 0.14 | 0.15 | 0.09 | 0.14 | 0.15 | 0.09 | 0.03 | 0.16 | 0.09 | | | |
| P.F. | 0.77 | 0.93 | 0.62 | 0.50 | 0.43 | 1.99 | 2.23 | 0.40 | 1.15 | 1.22 | 0.73 | 0.67 | 0.69 | 0.52 | 0.66 | 1.12 | 0.77 | 0.89 | 0.74 | 0.70 | 0.56 | 0.48 | 0.65 | | | |
| Total | 100.31 | 100.40 | 97.35 | 98.44 | 98.93 | 99.87 | 100.82 | 100.27 | 99.17 | 100.83 | 100.77 | 100.88 | 100.23 | 100.53 | 100.92 | 99.65 | 99.15 | 99.17 | 99.56 | 99.80 | 100.13 | 100.69 | 99.09 | | | |
| Fe ₂ O _{3t} | 3.70 | 4.00 | 3.19 | 2.29 | 1.18 | 6.41 | 6.56 | 0.57 | 2.90 | 6.19 | 3.27 | 1.58 | 2.30 | 2.16 | 2.89 | 2.9 | 1.88 | 2.84 | 1.90 | 1.68 | 0.95 | 2.4 | 1.93 | | | |
| Rb | 23 | 17 | 28 | 67 | 124 | 55 | 34 | 0.1 | 81 | 88 | 114 | 129 | 89 | 127 | 74 | 111 | 110 | 165 | 216 | 163 | 356 | 250 | 303 | | | |
| Sr | 310 | 322 | 297 | 184 | 144 | 496 | 599 | 904 | 376 | 526 | 354 | 311 | 507 | 262 | 342 | 617 | 643 | 282 | 280 | 193 | 77 | 280 | 59 | | | |
| Y | 20 | 38 | 15 | 29 | 27 | 14 | 15 | 8 | 14 | 22 | 19 | 8 | 13 | 15 | 11 | 15 | 11 | 10 | 12 | 12 | 41 | 26 | 41 | | | |
| Zr | 176 | 184 | 140 | 133 | 107 | 107 | 113 | 21 | 37 | 90 | 47 | 11 | 30 | 14 | 26 | 43 | 24 | 165 | 255 | 136 | 80 | 204 | 149 | | | |
| V | 34 | 31 | | | | | | | | | | | | | | | | 22 | 20 | 13 | 4 | 24 | 7 | | | |
| Sc | | | | | | | | | | | | | | | | | | | | | | | | | | |
| Ba | 852 | 642 | 619 | 968 | 1364 | 893 | 787 | 304 | 1121 | 1159 | 1025 | 1390 | 1459 | 971 | 1265 | 1058 | 891 | 968 | 1247 | 826 | 347 | 729 | 240 | | | |
| La | 26 | 26 | 28 | 31 | 85 | 34 | 27 | 13 | 40 | 58 | 44 | 68 | 32 | 64 | 78 | 51 | 17 | 57 | 113 | 49 | 33 | 80 | 39 | | | |
| Ce | 46 | 55 | 52 | 68 | 85 | 65 | 56 | 39 | 74 | 110 | 79 | 126 | 63 | 125 | 126 | 89 | 39 | 108 | 183 | 89 | 57 | 158 | 87 | | | |
| Pr | 5.3 | 6.9 | 6.9 | 8.8 | 6.8 | 6.2 | 5.2 | 7.0 | 12.0 | 12.0 | 8.8 | 12.7 | 6.2 | 13.0 | 9.8 | 3.9 | 3.6 | 12.0 | 19.0 | 9.3 | 5.8 | 16.0 | 9.6 | | | |
| Nd | 19 | 28 | 18 | 25 | 37 | 24 | 25 | 21 | 25 | 40 | 31 | 42 | 23 | 46 | 42 | 33 | 14 | 45 | 59 | 31 | 19 | 59 | 37 | | | |
| Sm | 3.1 | 5.7 | 2.9 | 5.0 | 5.8 | 3.8 | 4.7 | 3.3 | 4.0 | 6.5 | 5.0 | 5.0 | 3.9 | 8.0 | 6.5 | 4.9 | 2.5 | 7.5 | 6.7 | 4.9 | 4.3 | 10.0 | 8.9 | | | |
| Eu | 1.08 | 1.24 | 1.18 | 0.89 | 0.83 | 1.10 | 1.20 | 0.87 | 0.94 | 1.80 | 1.10 | 1.30 | 0.82 | 1.30 | 1.00 | 0.60 | 0.83 | 1.50 | 1.20 | 0.88 | 0.55 | 1.40 | 0.98 | | | |
| Gd | 3.2 | 6.2 | 6.2 | 0.36 | 0.74 | 3.4 | 3.5 | 2.3 | 3.0 | 6.0 | 4.3 | 3.2 | 3.0 | 6.7 | 4.4 | 3.9 | 2.1 | 5.7 | 3.8 | 3.8 | 5.1 | 6.9 | 7.1 | | | |
| Tb | | | | | | | | | | | | | | | | | | | | | | | | | | |
| Dy | 3.2 | 6.2 | 6.2 | 0.36 | 0.74 | 2.3 | 2.4 | 1.30 | 2.1 | 4.1 | 3.4 | 1.20 | 2.0 | 5.2 | 2.3 | 2.5 | 1.60 | 3.7 | 1.50 | 2.2 | 6.5 | 4.5 | 7.1 | | | |
| Ho | 0.67 | 1.34 | 0.49 | 1.22 | 0.68 | 0.49 | 0.51 | 0.24 | 0.46 | 0.83 | 0.71 | 0.22 | 0.42 | 1.10 | 0.43 | 0.51 | 0.32 | 0.71 | 0.27 | 0.43 | 1.60 | 0.95 | 1.5 | | | |
| Er | 1.82 | 3.89 | 1.51 | 3.91 | 2.05 | 1.33 | 1.18 | 0.66 | 1.4 | 2.4 | 2.1 | 0.56 | 1.1 | 3.1 | 1.1 | 1.5 | 0.94 | 1.9 | 0.7 | 1.2 | 5.2 | 2.7 | 4.6 | | | |
| Yb | 2.1 | 3.78 | 1.51 | 3.91 | 2.05 | 1.33 | 1.18 | 0.66 | 1.4 | 2.4 | 2.1 | 0.56 | 1.1 | 3.1 | 1.1 | 1.5 | 0.94 | 1.9 | 0.7 | 1.2 | 5.2 | 2.7 | 4.6 | | | |
| Lu | 0.30 | 0.54 | 0.24 | 0.66 | 0.34 | 0.19 | 0.19 | 0.08 | 0.19 | 0.29 | 0.26 | 0.08 | 0.13 | 0.38 | 0.13 | 0.17 | 0.14 | 0.22 | 0.09 | 0.17 | 0.85 | 0.39 | 0.73 | | | |
| Hf | 4.3 | 4.9 | 3.6 | 4.5 | 3.3 | 3.6 | 3.7 | 2.5 | 5.2 | 7.4 | 4.9 | 5.4 | 4.7 | 6.7 | 6.4 | 5.5 | 3.6 | 5.4 | 7.5 | 4.6 | 3.7 | 8.4 | 8.2 | | | |
| Ta | 0.31 | 0.34 | 0.28 | 1.17 | 1 | 0.6 | 0.26 | 0.21 | 0.54 | 0.71 | 0.88 | 0.3 | 0.96 | 0.27 | 0.17 | 1.8 | 0.99 | 1.00 | 0.85 | 0.87 | 3.3 | 2.2 | 3.0 | | | |
| Nb | 6.4 | 7.7 | 5.0 | 6.0 | 9.0 | 1.29 | 1.43 | 1.00 | 0.75 | 0.54 | 0.90 | 0.07 | 0.40 | 0.67 | 0.20 | 0.63 | 0.77 | 0.22 | 0.50 | 0.46 | 2.2 | 1.40 | 1.20 | | | |
| W | 1.02 | 0.93 | 6.7 | 8.4 | 6.0 | 9.7 | 19 | 7.1 | 23 | 20 | 30 | 57 | 18 | 34 | 32 | 32 | 63 | 30 | 43 | 48 | 50 | 45 | 48 | | | |
| Pb | 6.7 | 8.4 | 6.0 | 10.0 | 18.0 | 6.6 | 3.2 | 1.4 | 17 | 7.4 | 9.3 | 17 | 4.5 | 13 | 12 | 14.0 | 6.3 | 2.2 | 40 | 36 | 33.0 | 59 | 33 | | | |
| Th | 2.3 | 3.8 | 3.8 | 13.3 | 11.3 | 6.6 | 3.2 | 1.4 | 17 | 7.4 | 9.3 | 17 | 4.5 | 13 | 12 | 14.0 | 6.3 | 2.2 | 40 | 36 | 33.0 | 59 | 33 | | | |
| U | 0.35 | 0.64 | 0.49 | 1.70 | 1.30 | 1.00 | 0.63 | 0.19 | 2.5 | 0.88 | 1.80 | 0.69 | 0.68 | 2.03 | 1.02 | 2.6 | 3.3 | 1.4 | 1.60 | 4.0 | 2.9 | 8.9 | 6.8 | | | |
| Ni | 0.64 | 0.97 | 0.55 | 1.03 | 1.25 | 0.45 | 0.47 | 0.37 | 0.60 | 0.75 | 0.69 | 0.78 | 0.64 | 1.07 | 0.76 | 0.66 | 0.50 | 0.90 | 1.01 | 0.79 | 1.15 | 1.67 | 1.76 | | | |
| NYTSY | 0.17 | 0.20 | 0.20 | 0.61 | 0.57 | 0.69 | 0.36 | 0.09 | 0.76 | 0.69 | 0.69 | 0.56 | 0.46 | 0.59 | 0.47 | 1.04 | 0.67 | 0.92 | 1.45 | 1.10 | 2.1 | 2.2 | 1.77 | | | |

Table 2 (continued)

| | Late-shear ALK (Ki) | | | | | | | | | | Tinedjelalen ring complex | | | | | | | |
|---------------------------------|---------------------|-------|--------|---------|---------|---------|---------|---------|---------|--------|---------------------------|-------|----------|----------|----------|----------|-----------|----------|
| | Kidal ring-complex | | | | | | | | | | RB358-1 | | JPL306-2 | JPL347-2 | JPL325-4 | JPL326-4 | JPL345b-5 | JPL337-6 |
| | B20-1 | B60-2 | B186-4 | RB531-6 | RB455-7 | RB551-8 | RB549-1 | RB554-1 | JPL234- | | | | | | | | | |
| SiO ₂ | 64.51 | 75.13 | 72.10 | 76.36 | 75.03 | 77.00 | 75.43 | 72.11 | 75.98 | 73.00 | 67.45 | 70.35 | 72.44 | 75.23 | 69.71 | 74.72 | 76.19 | |
| TiO ₂ | 0.82 | 0.21 | 0.36 | 0.13 | 0.31 | 0.11 | 0.21 | 0.29 | 0.08 | 0.33 | 0.44 | 0.44 | 0.44 | 0.27 | 0.61 | 0.08 | 0.11 | |
| Al ₂ O ₃ | 15.60 | 12.22 | 13.22 | 12.28 | 12.60 | 12.13 | 12.25 | 13.32 | 11.99 | 13.17 | 15.57 | 14.12 | 13.47 | 12.76 | 13.67 | 10.90 | 11.31 | |
| Fe ₂ O ₃ | | | | | | | | | | | | | | | | | | |
| FeO | | | | | | | | | | | | | | | | | | |
| MnO | 0.20 | 0.08 | 0.07 | 0.04 | 0.05 | 0.04 | 0.06 | 0.05 | 0.01 | 0.13 | 0.14 | 0.11 | 0.07 | 0.04 | 0.07 | 0.02 | 0.05 | |
| MgO | 0.64 | 0.01 | 0.23 | 0.01 | 0.05 | 0.01 | 0.01 | 0.03 | 0.01 | 0.15 | 0.11 | 0.20 | 0.46 | 0.29 | 0.65 | 0.02 | 0.03 | |
| CaO | 1.45 | 0.31 | 0.77 | 0.24 | 0.36 | 0.07 | 0.03 | 0.33 | 0.06 | 0.32 | 0.35 | 0.28 | 1.07 | 0.72 | 1.10 | 0.61 | 0.37 | |
| Na ₂ O | 5.06 | 3.92 | 3.96 | 3.67 | 3.50 | 3.49 | 3.98 | 4.01 | 4.33 | 4.69 | 5.53 | 5.07 | 3.78 | 3.70 | 4.22 | 4.44 | 4.68 | |
| K ₂ O | 5.81 | 5.12 | 4.98 | 4.76 | 5.30 | 4.91 | 5.28 | 5.64 | 4.22 | 5.20 | 6.02 | 5.53 | 5.10 | 4.84 | 3.90 | 4.34 | 4.19 | |
| P ₂ O ₅ | 0.23 | 0.01 | 0.04 | 0.02 | 0.01 | 0.01 | 0.01 | 0.01 | 0.10 | 0.07 | 0.03 | 0.07 | 0.10 | 0.07 | 0.14 | 0.01 | 0.02 | |
| P.F. | 0.50 | 0.29 | 0.51 | 0.36 | 0.52 | 0.38 | 0.35 | 0.31 | 0.51 | 0.52 | 0.63 | 0.48 | 0.45 | 0.56 | 1.03 | 0.61 | 0.61 | |
| Total | 99.12 | 99.72 | 98.95 | 99.15 | 99.46 | 99.28 | 100.02 | 98.58 | 98.72 | 100.05 | 100.06 | 99.76 | 99.95 | 100.20 | 98.68 | 98.49 | 100.12 | |
| Fe ₂ O _{3t} | 4.53 | 2.55 | 2.85 | 1.35 | 1.82 | 1.19 | 2.54 | 2.61 | 1.51 | 2.60 | 3.99 | 3.27 | 2.70 | 1.81 | 3.77 | 2.88 | 2.69 | |
| Rb | 52 | 128 | 111 | 213 | 174 | 191 | 182 | 160 | 194 | 96 | 94 | 84 | 139 | 167 | 109 | 426 | 570 | |
| Sr | 42 | 15 | 97 | 55 | 60 | 43 | 20 | 39 | 8 | 20 | 24 | 18 | 125 | 86 | 197 | 28 | 10 | |
| Y | 55 | 74 | 51 | 65 | 64 | 52 | 112 | 61 | 191 | 61 | 116 | 50 | 62 | 49 | 82 | 241 | 280 | |
| Zr | 192 | 572 | 441 | 139 | 250 | 137 | 581 | 550 | 371 | 490 | 399 | 344 | 316 | 227 | 534 | 847 | 903 | |
| V | | 3.98 | 18.42 | 7.87 | | 3.31 | 4.33 | 9.37 | | 5.17 | 1.51 | 5.61 | 32 | 19 | 56 | 0.97 | 2.42 | |
| Sc | 15.6 | | | | 3.7 | | | | 0.32 | | | | | | | | | |
| Ba | 1588 | 173 | 604 | 250 | 449 | 333 | 479 | 340 | 73 | 174 | 293 | 146 | 674 | 453 | 849 | 25 | 17 | |
| La | 44 | 109 | 69 | 42 | 57 | 57 | 204 | 85 | 43 | 123 | 806 | 148 | 61 | 44 | 84 | 63 | 55 | |
| Ce | 94 | 211 | 143 | 90 | 120 | 118 | 375 | 164 | 105 | 239 | 1321 | 287 | 120 | 95 | 155 | 122 | 130 | |
| Pr | | 23.9 | 15.9 | 9.7 | | 12.1 | 40 | 18.6 | | 26.1 | 141 | 32 | 14.0 | 10.5 | 18.0 | 16.0 | 15.4 | |
| Nd | 48 | 86 | 58 | 33 | 48 | 39 | 137 | 65 | 77 | 90 | 485 | 109 | 51 | 37 | 66 | 59 | 56 | |
| Sm | 9.4 | 15.3 | 10.2 | 6.9 | 8.9 | 6.9 | 22.5 | 10.9 | 29.2 | 13.9 | 59 | 15.9 | 9.1 | 7.3 | 12.2 | 16.1 | 16.6 | |
| Eu | 4.82 | 0.89 | 1.20 | 0.29 | 0.62 | 0.30 | 0.93 | 0.72 | 0.64 | 0.72 | 1.80 | 0.96 | 1.12 | 0.73 | 1.52 | 0.54 | 0.63 | |
| Gd | | 13.1 | 8.7 | 6.6 | | 5.8 | 18.0 | 9.8 | 38 | 10.5 | 38 | 11.4 | 8.8 | 6.8 | 12.4 | 20.8 | 20.9 | |
| Tb | 1.3 | | | | 1.3 | | | | 6.9 | | | | | | | | | |
| Dy | | 12.0 | 8.3 | 8.7 | | 6.9 | 16.8 | 9.6 | | 9.7 | 24.3 | 9.0 | 9.2 | 7.5 | 12.2 | 29.2 | 34.7 | |
| Ho | 1.6 | 2.50 | 1.71 | 1.94 | 1.8 | 1.51 | 3.3 | 1.99 | 7.8 | 1.94 | 4.5 | 1.73 | 1.95 | 1.55 | 2.61 | 6.8 | 8.0 | |
| Er | | 7.1 | 4.8 | 6.0 | | 4.7 | 9.1 | 5.6 | | 5.3 | 9.6 | 4.5 | 5.7 | 4.6 | 7.3 | 21.2 | 25.7 | |
| Yb | 4.0 | 7.4 | 4.9 | 6.8 | 5.9 | 5.3 | 9.5 | 6.1 | 16.4 | 5.2 | 9.3 | 4.9 | 5.8 | 4.8 | 7.3 | 22.3 | 25.9 | |
| Lu | 0.65 | 1.16 | 0.77 | 1.04 | 0.99 | 0.83 | 1.45 | 0.88 | 2.3 | 0.83 | 1.57 | 0.78 | 0.82 | 0.75 | 1.05 | 3.06 | 3.72 | |
| Hf | 5.3 | 14.1 | 10.2 | 5.8 | 9.3 | 5.6 | 14.7 | 13.9 | 18.8 | 10.6 | 8.1 | 8.0 | 8.8 | 6.8 | 13.1 | 33.6 | 34.5 | |
| Ta | 0.76 | 1.32 | 1.01 | 2.14 | 1.65 | 1.64 | 1.46 | 1.05 | 3.3 | 1.21 | 1.18 | 1.14 | 1.38 | 1.32 | 1.00 | 6.1 | 6.9 | |
| Nb | 12.0 | 22.4 | 16.6 | 24.3 | 19.0 | 17.3 | 20.8 | 17.3 | 30 | 21.3 | 30 | 19.7 | 22.1 | 15.9 | 21.7 | 81 | 82 | |
| W | | 0.49 | 0.72 | 1.48 | | 0.92 | 0.82 | 0.97 | | 0.42 | 0.64 | 0.31 | 0.62 | 0.17 | 2.42 | 3.5 | 1.62 | |
| Pb | 11.0 | 19.0 | 15.6 | 20.8 | 27.0 | 20.9 | 15.6 | 14.4 | 53 | 16.2 | 19.4 | 20.5 | 20.6 | 18.2 | 16.8 | 40 | 66 | |
| Th | 3.4 | 15.4 | 13.0 | 23.6 | 17.0 | 21.7 | 27.9 | 21.5 | 27.4 | 10.7 | 14.2 | 10.4 | 13.6 | 18.0 | 9.8 | 59 | 41 | |
| U | 0.5 | 3.0 | 2.6 | 5.8 | 3.9 | 5.0 | 6.8 | 4.1 | 6.3 | 2.4 | 2.0 | 2.0 | 3.1 | 4.8 | 1.8 | 15.9 | 18.7 | |
| NYTS X | 1.06 | 3.2 | 1.90 | 1.97 | 2.09 | 2.01 | 4.4 | 2.32 | 5.6 | 2.36 | 4.9 | 1.94 | 1.75 | 1.63 | 2.27 | 6.3 | 7.1 | |
| NYTS Y | 0.42 | 0.81 | 0.73 | 1.28 | 1.00 | 1.07 | 1.26 | 1.02 | 1.56 | 0.69 | 0.89 | 0.69 | 0.89 | 0.99 | 0.67 | 3.3 | 3.6 | |

index (AI; molar Na + K/Al; Fig. 5D) clearly separates the alkaline group (AI > 0.87; Liégeois, 1988) including peralkaline facies (AI > 1) from the calc-alkaline groups which have AI < 0.87. The latter group includes the YT and shoshonitic series, which are very close in that diagram. Only very few HKCA samples have an apaitic index above 0.87, as is the case for the peculiar Takarakoum pluton due to high Na₂O content (Fig. 5C). The alkaline series is then characterized by low Al and high Na₂O contents while the high K₂O content of the shoshonitic series is balanced by a low Na₂O content (Fig. 5A,C).

CaO varies also progressively from the active margin-related group through the HKCA groups,

with the extreme position taken by the YT trend and shoshonitic series, to the alkaline group, the poorest in CaO (Fig. 6A,B). A ternary diagram combining K₂O, Na₂O and CaO (Fig. 6C) displays the large zone covered by the Tuareg shield magmatism from the active margin calcic series to the post-collisional alkaline group.

Concerning trace elements, the HFSE vs. FeOt/MgO diagram (Whalen et al., 1987; Fig. 6D) gives interesting information, even if the A-type classification is only partly applicable here. The alkaline group falls mainly within the A-type field and is the only group displaying large enrichment of the FeOt/MgO ratio. The HKCA and shoshonitic

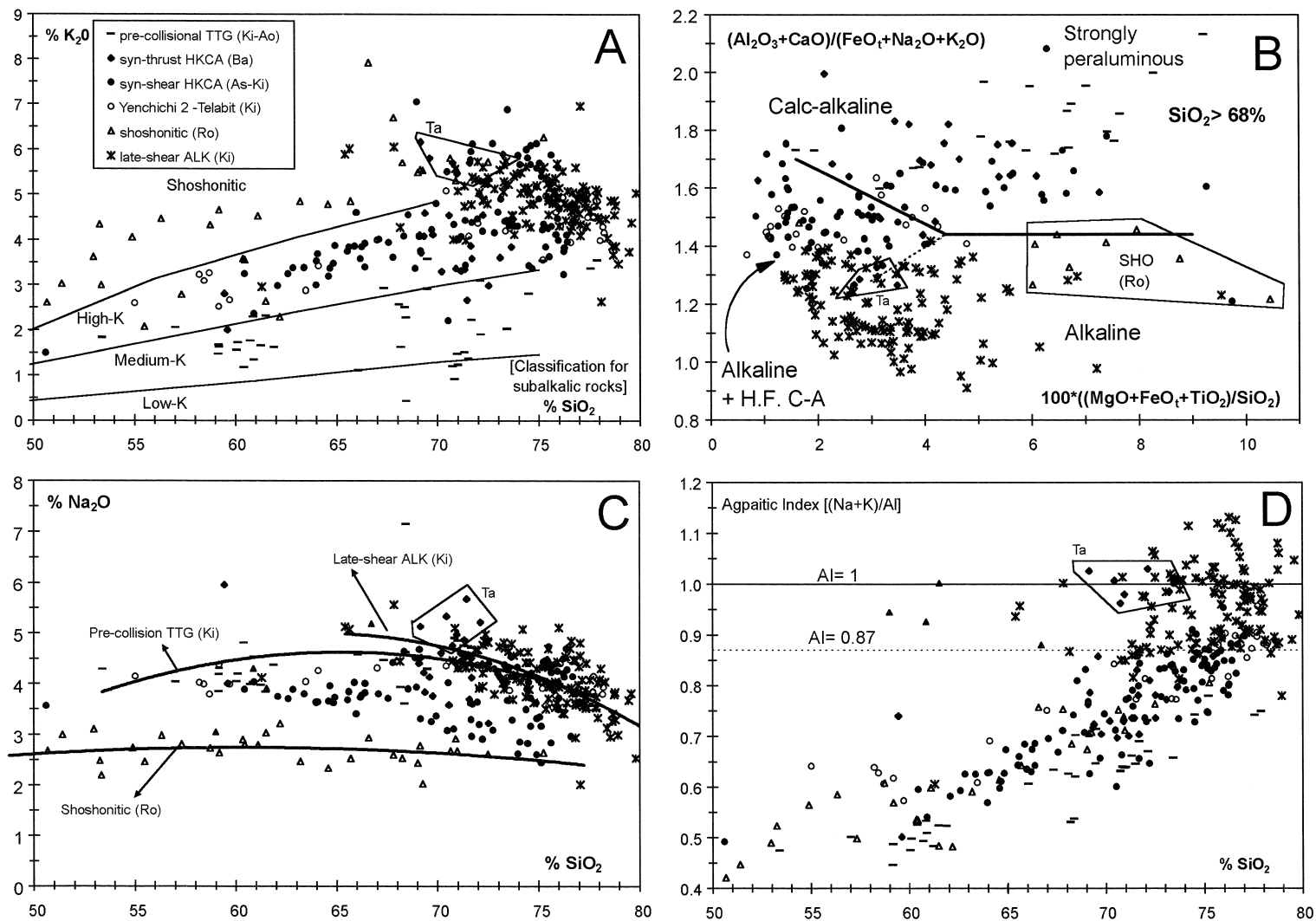


Fig. 5. Major element variations of the different studied series. (A) SiO₂ vs. K₂O (boundaries from Peccerillo and Taylor, 1976); (B) Major element discrimination of post-collisional granites (SiO₂ > 68%) from Sylvester (1989); (C) SiO₂ vs. Na₂O; (D) SiO₂ vs. agpaitic index: peralkaline rocks have an agpaitic index > 1 while other alkaline rocks are generally above 0.87 (Liégeois and Black, 1987). TTG = tonalite-trondhjemite-granodiorite; HKCA = high-K calc-alkaline; ALK = alkaline; Ao = Aouzegueur terrane; Ba = Barghot terrane; Ki = Kidal terrane (for localization of these terranes, see Fig. 1); Ro = Romania (Tismana pluton; Duchesne et al., 1998).

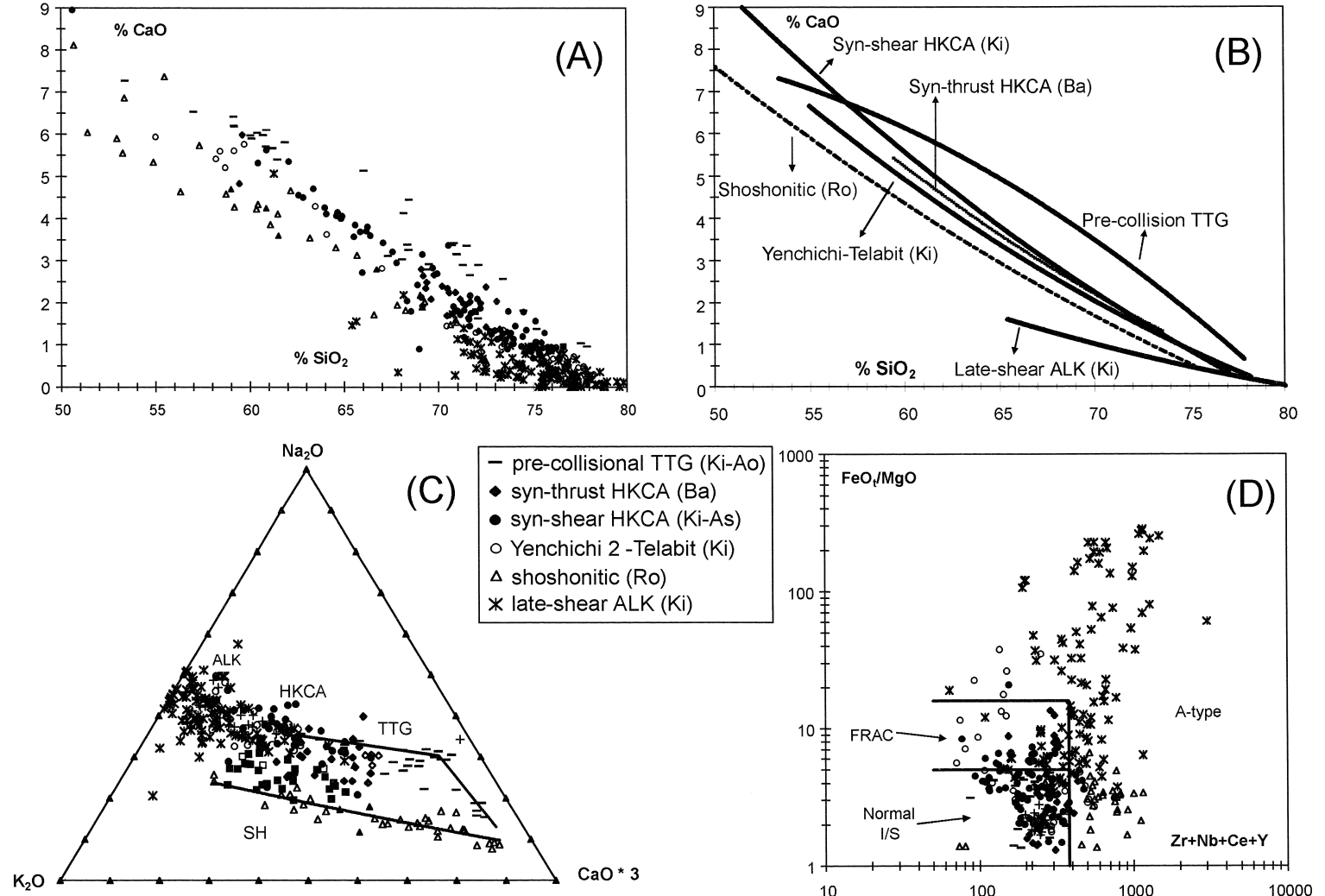


Fig. 6. Major and trace element variations of the different studied series. (A) SiO₂ vs. CaO; (B) SiO₂ vs. CaO, schematic trends; (C) K₂O-Na₂O-3*CaO triangle; (D) Zr+Nb+Ce+Y vs. FeO₇/MgO discrimination diagram (Whalen et al., 1987). Abbreviations are as in Fig. 5.

groups display similar trends characterized by an early increase of HFSE with increasing FeOt/MgO, i.e., with increasing differentiation. Later on, the decrease of these elements results in shoulder-type trends. This is mainly due to the saturation in zircon at intermediate compositions. As a consequence, intermediate rocks, particularly from the shoshonitic series, can be located within the A-type field, the end of the differentiation trend being in the I/S field. The YT group even attains again the A-type field at low Zr + Nb + Ce + Y and high FeOt/MgO values, which appears to be an extreme HKCA trend. In the middle of the diagram (X between 200 and 400, Y between 3 and 8) lies a zone where all groups have representatives.

The concentration of Zr at which the saturation in zircon occurs can be used to determine the temperature of this saturation, taking into account the whole-rock chemistry (Watson and Harrison, 1983). These calculations show that the alkali content is correlated to the saturation temperature, allowing a larger enrichment in Zr and associated elements in alkali-rich rocks. The TTG and syn-thrust HKCA series give saturation temperature in the range 750–800°C, except the Takarakoum pluton (> 800°C), which is richer in Na₂O (Fig. 5C). This latter fact confirms that the higher Na content in this pluton is primary and not linked to a late albitization, not seen in thin section. The syn-shear HKCA group, although more scattered (it concerns 10 plutons), indicates a similar temperature range of 750–800°C. The Telabit dyke swarm shows a higher zircon saturation temperature of 800–850°C. In the alkaline series, lavas are hot (1000°C), the dykes and some plutonic rocks are in the range 800–850°C while some rings from both the Kidal and Timedjelalen complexes have lower calculated zircon saturation temperatures, although still high, between 750 and 800°C. The zircon saturation temperature of the Tismana shoshonitic series is quite high, between 850 and 900°C (Duchesne et al., 1998).

These results are in agreement with experimental constraints that predict a temperature > 830°C and possibly > 940°C for A-type granites, exceeding those of S- and I-type granites of similar silica content (750–850°C). This suggests a different origin for these two groups of granites (Clemens et al., 1986). Whatever the internal variations and the con-

sidered series, there is a tendency of increasing magma temperatures at the end of the orogeny, which is a main point to be solved (Sylvester, 1989).

6. Sliding normalization: a tool to compare magmatic series

All the previous geochemical diagrams (Figs. 5 and 6) not only indicate that important differences exist between the considered groups, but also that the transition between them is not precisely defined due to large overlap. Moreover, they also show the importance of considering *series*, not only samples. This raises the problem of comparing rocks at different stages of differentiation, and leads us to propose a ‘sliding normalization’. This means that the normalization is done with respect to a reference series and not only to a reference sample.

The concept of the sliding normalization is simple. For a reference series, the chemical variation trends as a function of SiO₂ are fitted to a second-order polynomial. For any sample under study, the concentration of an element is normalized to the calculated concentration in the reference series at the same silica content as the sample (Fig. 7).

Although the choice of the reference series does not alter the relative position of the studied samples, it is desirable to use a real liquid line of descent in

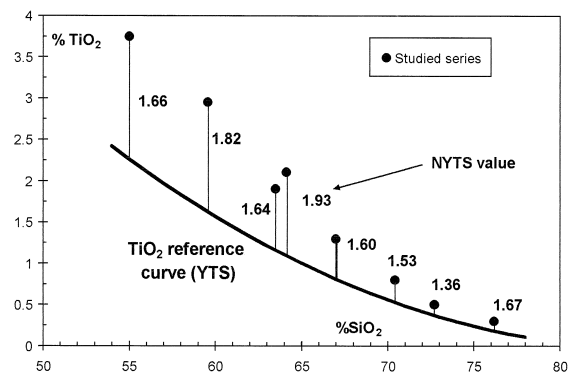


Fig. 7. Principle of sliding diagrams: each studied sample is normalized to the sample from the idealized reference series (here the Yenchichi 2-Telabit series) which has the same SiO₂ content. This allows the comparison of rocks with variable silica contents, i.e., to compare series. The curve is characterized by a second order equation (see Fig. 9). NYTS = normalized to the Yenchichi 2-Telabit series.

the range of the studied series, to amplify the differences. In this study, we use the Yenchichi 2-Telabit (YT) series that meets these requirements. The Telabit huge dyke swarm (Fig. 3A) defines a long although simple liquid line of descent from 54 to 71% SiO₂ (Liégeois, 1988) and is extended up to

77% SiO₂ by the contemporaneous Yenchichi 2 high-level pluton. (Fig. 8A,B). The second-order polynomial normalisation values calculated for each element by least-squares regression are listed in Table 3. The sliding normalization values relatively to the Yenchichi 2-Telabit series (normalized to the

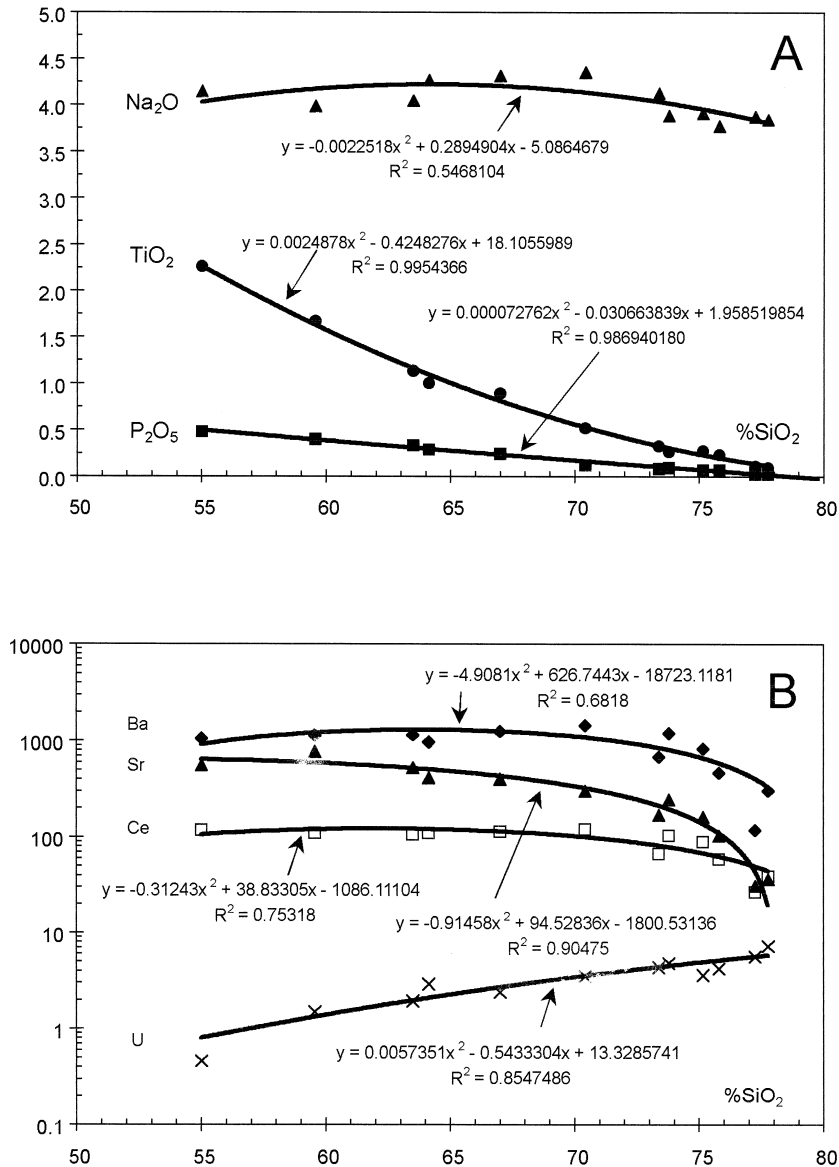


Fig. 8. Examples of the normalized evolution trends of some elements from the Yenchichi 2-Telabit (YT) series and of the resulting second order polynomial. (A) YT curves for some major elements: Na₂O, TiO₂ and P₂O₅; (B) YT curves for some trace elements: Ba, Sr, Ce and U.

Table 3

Parameters of the second order curves of the Yenchichi-Telabit series used for the sliding normalization ($y = ax^2 + bx + c$, where $x = \text{SiO}_2$) [value of SiO_2 on an anhydrous basis]^a

| | <i>a</i> | <i>b</i> | <i>c</i> |
|---------------------------------|-------------|-----------|----------|
| TiO ₂ | 0.0024941 | -0.42558 | 18.126 |
| Al ₂ O ₃ | -0.014407 | 1.7917 | -39.742 |
| Fe ₂ O _{3t} | 0.011466 | -1.9536 | 83.528 |
| MnO | 0.00023421 | -0.036233 | 1.4486 |
| MgO | 0.0033775 | -0.61434 | 27.438 |
| CaO | 0.0020147 | -0.53127 | 29.521 |
| K ₂ O | -0.0033766 | 0.54241 | -17.357 |
| Na ₂ O | -0.0022865 | 0.29407 | -5.2362 |
| P ₂ O ₅ | -0.0016068 | 1.045835 | -21.744 |
| Rb | 0.18803 | -20.092 | 617.37 |
| Nd | -0.091839 | 10.592 | -252.91 |
| Y | 0.014658 | -2.5965 | 138.7 |
| Sm | -0.012219 | 1.32609 | -26.513 |
| Yb | 0.0031057 | -0.44376 | 18.607 |
| Ba | -4.9333 | 630.01 | -18828 |
| Sr | -0.92515 | 95.905 | -1845.1 |
| Ce | -0.31347 | 38.966 | -1090.3 |
| Eu | -0.00056961 | -0.020974 | 5.4292 |
| Zr | -0.72551 | 85.895 | -2199.7 |
| Nb | -0.03139 | 3.9642 | -107.43 |
| Hf | -0.013993 | 1.6861 | -42.892 |
| Ta | -0.001608 | 0.23021 | -6.982 |
| V | 0.17092 | -32.452 | 1494 |
| Pb | -0.021974 | 3.4535 | -114.53 |
| Th | 0.0053248 | 0.079569 | -17.334 |
| U | 0.0056899 | -0.53729 | 13.133 |
| A. I. | 0.000261 | -0.022443 | 1.04446 |
| P. I. | 0.00073041 | -0.13741 | 6.316 |

^aA spreadsheet prepared for the sliding normalization calculations can be obtained from the first author.

Yenchichi 2-Telabit series, NYTS) can be displayed in several types of diagrams, including spidergrams.

7. Sliding NYTS diagrams applied to high-K calc-alkaline versus alkaline magmatism

The NYTS normalization fulfils its expected role: the spectra within each group are similar whatever the SiO_2 content. Only some very differentiated samples (> 75% SiO_2), where larger variations can occur due to small absolute abundances of many trace elements, show peculiar features. For this reason the SiO_2 -rich samples JPL280, BLN15, JPL252, JPL414 (Table 2) as well as the alkaline B20 syenite which represents feldspar cumulate have not been included in the spidergrams, for clarity.

The observed variations of the *syn-shear HKCA YT reference* group (Fig. 9A) give the expected natural variability compared to the mathematical model. The *pre-collisional TTG* group (Fig. 9B) shows depletion in all elements except Sr, Ca and Fe. The *syn-thrust* groups (Fig. 9C) display spectra close to the pre-collisional TTG group, with more Sr and lower mean Fe. The Takarakoum pluton, which is particularly rich in alkalis for this group and has as a consequence an ambiguous major element signature (Fig. 5), is not different from the other plutons. The *syn-shear HKCA* group displays rather flat patterns (Fig. 9D). On average, they are enriched in Rb, Th, and U and partly in Ta, while they are depleted in HFSE elements (from Zr to Yb). The *late-shear alkaline* group (Fig. 9E) is not enriched in LILE (large ion lithophile elements, left of the diagram), but enriched in HFSE (high field strength elements, right of the diagram) and may present large depletions in Ba and Sr. The two samples richer in LILE belong to the last ring of the Timedjelalen ring complex (ring T6) and are also particularly rich in HFSE. The Tismana *shoshonitic* series (Duchesne et al., 1998; Fig. 9F) shows important enrichment in LILE and in HFSE, which accounts for its apparent A-type character (Fig. 6D; Duchesne et al., 1998).

It emerges from these NYTS spidergrams that two groups of elements are particularly useful: Zr, Hf, Y and REE on the one hand and Rb, Th, U, Nb and Ta on the other hand. Ba and Sr are not considered here because they are too dependent on feldspar fractionation. The presence of important troughs in the spidergrams for these elements is probably typical of the alkaline series, although they must not necessarily be present.

To simplify the comparison between groups, bivariate diagrams of normalized values can be constructed. It has been chosen to plot the mean of (Zr, Y, Ce, Sm, Yb)_{NYTS} vs. mean of (Rb, Th, U, Ta)_{NYTS}. Choosing the *mean* has two benefits: (1) Each element has a similar weight. This is mainly due to the normalization, but also to the fact that enrichment or depletion will affect all the elements among each group to largely the same extent. This avoids for example the excessive weight of Zr in the diagram of Whalen et al. (1987; Fig. 6D); (2) If an element is lacking in the studied series, the NYTS mean values of the other elements can be plotted, albeit with a

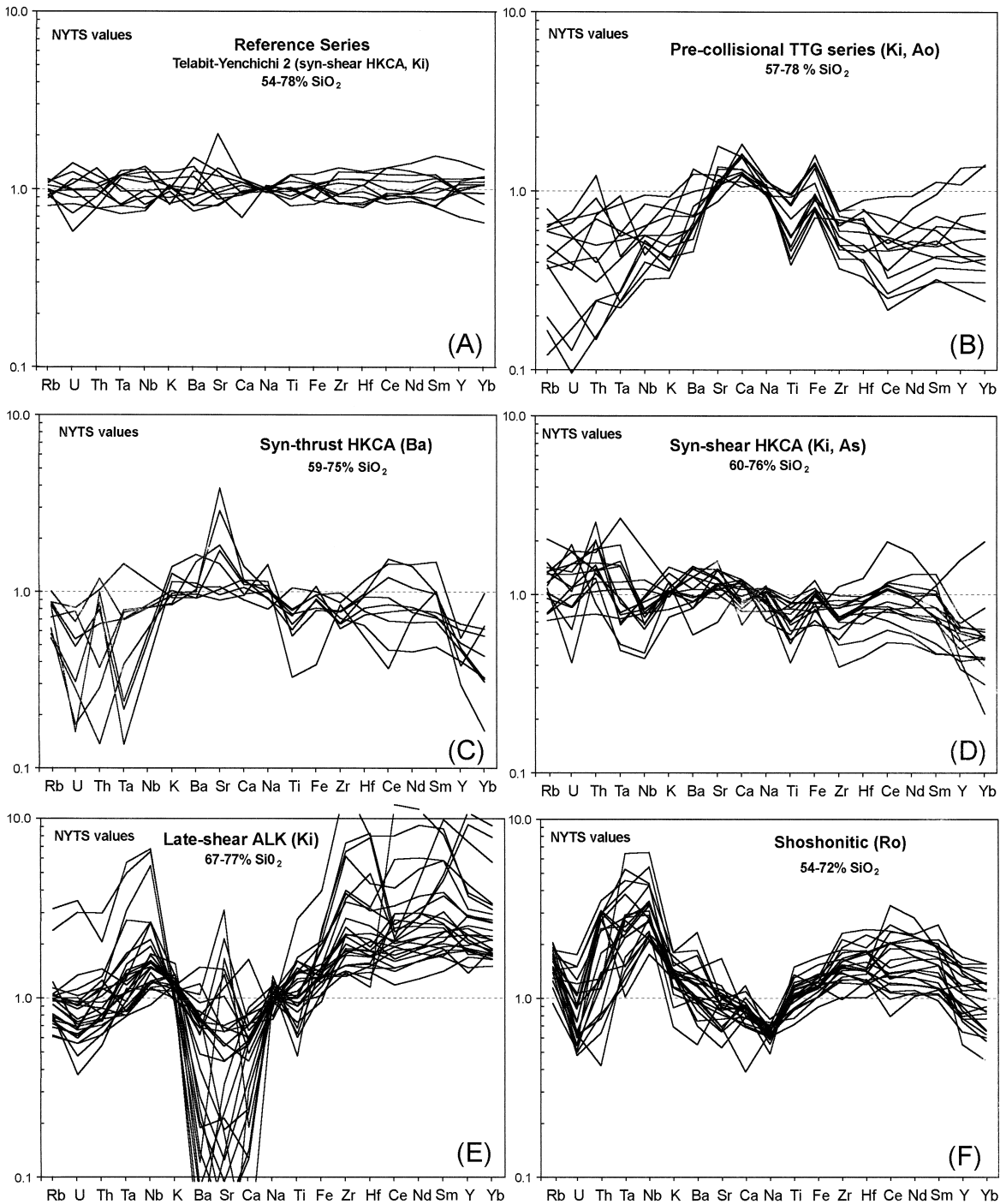
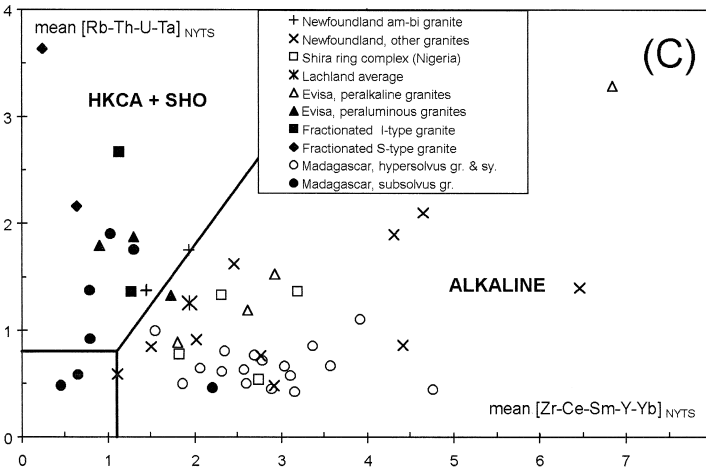
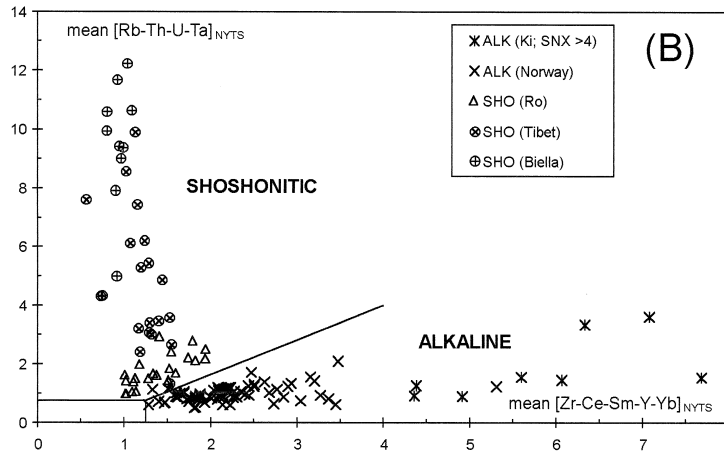
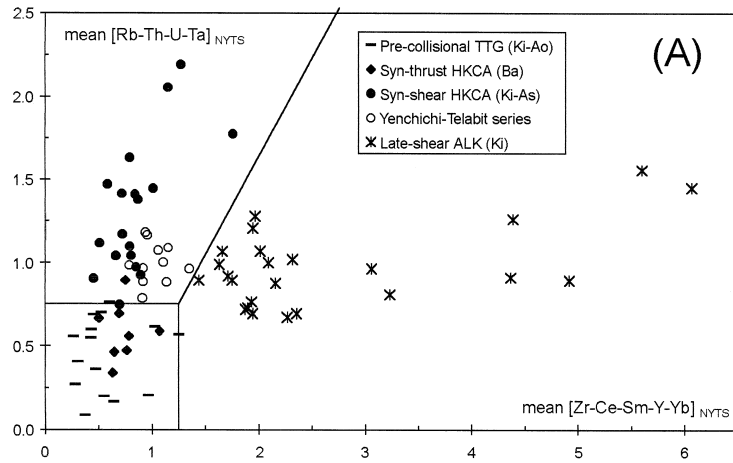


Fig. 9. Spidergrams normalized to the Yenchichi 2-Telabit series (NYTS, sliding normalization), showing the enhancement of the difference between series and the similarity of spectra in a given series irrespective of the silica content. (A) Yenchichi 2-Telabit reference series; (B) Pre-collisional TTG series; (C) Syn-thrust HKCA series; (D) Syn-shear HKCA series; (E) Late-shear alkaline series; (F) Shoshonitic Tismana series (data from Duchesne et al., 1998). For abbreviation, see Fig. 5.



NYTS= Normalization to the Yenchichi-Telabit series

decrease of the confidence level. However, the use of means requires that each element type be adequately weighted. For this reason, only three REE have been selected (one LREE, one MREE and one HREE) and only one element from the diadochic pairs Zr–Hf and Nb–Ta (one can be replaced by the other, Table 3). The two axes will be called SNX and SNY (sliding normalized X and Y).

In the bivariate SNY-SNX diagram (Fig. 10A), the alkaline and HKCA groups are distinct: for similar SNY values, the alkaline group has higher SNX values, forming a trend subparallel to the X-axis. The pre-collisional TTG group, including the most differentiated samples, lies close to the origin, with SNX and SNY values below 1. The syn-shear HKCA group has SNX values below 1.5 and SNY values between 0.8 and 1.7. The alkaline group reaches a SNX value of 6 while the SNY values are below 2. Two samples from the last venue of the Timedjelalen ring complex attain values of SNX around 7 and of SNY around 3.5 (Fig. 10B). Lines have been drawn to roughly separate three fields: the field of subduction-related granitoids, which includes the syn-thrust HKCA, the syn-shear HKCA and alkaline field. These lines will be particularly useful as reference when plotting other series.

In order to test the validity of these two different trends defined by the post-collisional Pan-African magmatism, some shoshonitic and alkaline well-studied series from outside the Tuareg shield have been plotted in the NYTS binary diagram. For the potassic group, we have chosen a shoshonitic series from Tibet (Turner et al., 1996) and the Traversella-Biella shoshonitic plutons from Italy (Bigioggero et al., 1994; Vander Auwera and Horion, 1998) in addition to the Romanian shoshonites. For the alkaline rocks, we have plotted the post-collisional A-type charnockitic series from Norway forming a constrained liquid line of descent from 50 to 76% SiO₂ (Duchesne and Wilmart, 1997). These reference se-

ries clearly illustrate the opposite variation trends of the potassic and of the alkaline series (Fig. 10B). Highly shoshonitic rocks can reach SNY values of 12 while with more or less constant low SNX values. Alkaline series have SNX values increasing much more rapidly than SNY values.

The position of the reference plutons of Whalen et al. (1987) in this diagram conforms to the Tuareg alkaline series (Fig. 10C). The different A-type series form different trends elongated in the alkaline domain, while fractionated I and S type series (both S and I granites type being HKCA in composition; Roberts and Clemens, 1993) lie in the calc-alkaline field. It has to be noted that the Evisa peraluminous granites (Bonin et al., 1987) are closer to the S-type representatives and do not follow the alkaline-peralkaline trend. Although the origin of these rocks is not yet fully understood, they probably do not belong to the main alkaline-peralkaline series (Bonin, pers. comm.). The Pan-African stratoid granitoids from Madagascar are post-collisional but present the particularity to be emplaced as a thick sequence of sheets mainly alkaline in composition (Nédélec et al., 1995). In the SNX-SNY diagram (Fig. 10C), the hypersolvus granites and syenites form an alkaline trend while the subsolvus granites determine a potassic trend. As we will see below, this suggests two different sources, not two different tectonic settings.

Rather than divergent, the potassic and alkaline trends are converging within the SNX-SNY diagram. They converge with increasing differentiation to the origin of the diagram, to the zone where the pre-collisional and syn-thrust groups are located. This can be seen when plotting the SNY and SNX parameters vs. silica (Fig. 11): the SNY parameter (Fig. 11A), during differentiation, is slightly decreasing in the shoshonitic Tismana and Tibet series, clearly decreasing within the Biella shoshonitic series and rather constant and low in the alkaline series; the SNX parameter (Fig. 11B) is relatively constant and

Fig. 10. SNX-SNY (sliding normalization X and Y) diagram opposing the mean of the NYTS values characteristics for the alkaline-peralkaline series (SNX) and for the high-K calc-alkaline-shoshonitic series (SNY). (A) Plot of the HKCA and alkaline series from the Tuareg shield. For abbreviation, see Fig. 5; (B) Other shoshonitic and alkaline series: Tismana shoshonitic series, Romania (Duchesne et al., 1998); shoshonitic lavas from Tibet (Turner et al., 1996); Biella shoshonitic pluton (Italy; Vander Auwera and Horion, 1998); Bjerkreim-Sokndal charnockitic A-type series (Norway; Duchesne and Wilmart, 1997). (C) Other reference series taken from Whalen et al. (1987 and references therein) except Madagascar from Nédélec et al. (1995). The reference lines have the following coordinates: (SNX, SNY): (0, 0.75); (1.25, 0.75); (1.25, 0); (4, 4).

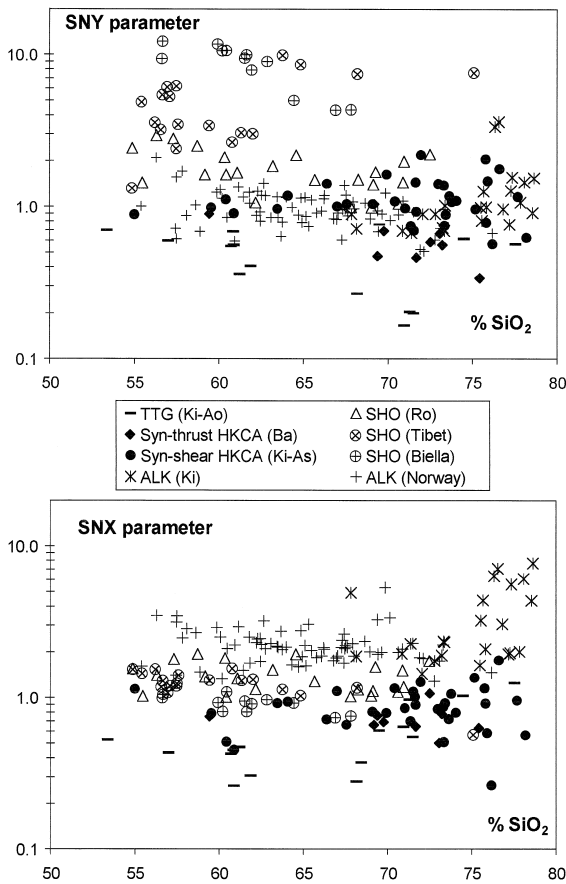


Fig. 11. Silica versus SNX and SNY parameters, showing that SNX and SNY of the series are similar all over the differentiation. This is then interpreted as a primary feature and not a differentiation-induced characteristic. Differentiated alkaline rocks show more variable values, a typical feature for these rocks.

low in the different calc-alkaline series (although at different levels) and more variable and more enriched in the alkaline series. This indicates that, except for some alkaline silica-rich samples that are high in the SNX parameter, the enrichment relatively to the YT series of the considered elements is not due to the differentiation, which does not substantially affect the two parameters. Differentiation even reduces the differences which exists in the less evolved, more basic rocks, due to the saturation and crystallisation of different minerals. This indicates that the observed differences are linked to the sources themselves, as it has been demonstrated for the K_2O

content of the Tibetan shoshonites (Turner et al., 1996).

8. Two distinct mainly juvenile sources for high-K calc-alkaline (HKCA)-shoshonitic and alkaline-peralkaline series

Judging from field relationships, HKCA and alkaline series appear to belong to different environments and, when present in the same region, they are generally successive and not strictly contemporaneous. Moreover, the later alkaline magmatism is hotter than the HKCA magmatism (zircon saturation temperature, this study; Clemens et al., 1986). This suggests two distinct sources generating magmas under different conditions. This can be attributed either to melting of a more mafic crustal source at higher temperature for alkaline rocks, leaving unsolved the problem of the extra-heat source (Sylvester, 1989), or to two distinct mainly mantle sources (Liégeois and Black, 1987; Bonin, 1990), implying a liquid line of descent and thereby suggesting the location of the complementary mafic rocks, which must be present in large volume, at the mantle–crust boundary.

HKCA batholiths are volumetrically important but are not ubiquitous. They are absent from the anorogenic period (intraplate setting) as well as from frontal collision (Glazner, 1991). They are relatively rare in oceanic domains and in cordilleran subduction zones: these environments rather comprise abundant low- and medium-K calc-alkaline magmatism. HKCA batholiths typically occur in post-collisional setting during large relative movements of terranes along major shear zones, more or less directly driven by oblique subduction. The large volumes can be attributed to the long duration of this process, often exceeding 50 Ma (Liégeois et al., 1994) and to the releasing bends in the strike-slip faults which create favourable conditions for more or less passive emplacement of the batholiths (Glazner, 1991). HKCA magmatism can then be very abundant but is not ubiquitous.

On the contrary, alkaline magmatism is present nearly everywhere, but generally in small amounts. It occurs in oceans and on continents, during subduc-

tion, orogeny and anorogenic periods. It seems however to be linked to deep lithospheric faults accompanied by short movements, allowing the tapping of a deep source, in oceanic island arcs (DeLong et al., 1975), in rifts (Bonin and Lameyre, 1978), in post-collisional setting (Boullier et al., 1986) or elsewhere (Black et al., 1985). Alkaline magmatism can sometimes be volumetrically important as in the Iforas (Fig. 3B), but will rarely last for a long period in a given area. Apparent long lasting alkaline provinces are rather a succession of small and short episodes (Vail, 1989). The voluminous anorogenic anorthosite-bearing alkaline Air province (Fig. 2B) occurred in less than 10 Ma (Moreau et al., 1994). The two preferred times for alkaline magmatism are however the intraplate and the end of post-collisional periods. These two phases are rarely followed by a period of important erosion, which explains why alkaline magmatism is most often seen through its volcanic or subvolcanic manifestations.

It seems then that the generation of HKCA and alkaline magmas is linked to different conditions that converge in some post-collisional settings. Indeed, HKCA series evolve at the end of their life to particularly enriched potassic facies, occasionally shoshonitic, whose volumes are always minor. Alkaline magmatism is not always present in post-collisional settings, but when it occurs it is very similar to true anorogenic alkaline manifestations (Black et al., 1985; Sylvester, 1989).

Isotopically, both series in the Tuareg shield result from an interaction between juvenile material, and an old continental crust (Fig. 4). Pb isotopes have indicated that mantle sources for HKCA and alkaline magmatism in the Adrar des Iforas had to be different (Liégeois, 1988). The old crustal interaction is not at the cause of the potassium enrichment. NYTS diagrams (Fig. 10) indicate that the whole series, from mafic to felsic rocks has common geochemical characteristics, whatever their isotopic signature. The syn-shear group, comprising samples from both Kidal and Assodé terranes, have similar geochemistry (Fig. 9D) despite different amounts of contamination by an old crust (Fig. 4). The important K-enrichment of the shoshonitic series of Tismana is already prominent at the beginning of the liquid line of descent at more than 1100°C and the contamination by an old crust evidenced by Nd and Sr isotopes

has no large geochemical effect on it (Duchesne et al., 1998). In the Tuareg shield, the late most K-enriched facies are also those which have the most juvenile isotopic signature (Liégeois and Black, 1987; Liégeois, 1988). This confirms that the K-enrichment must be related to the composition of the juvenile source. The problem to distinguish between a mantle source and a young lower mafic crustal source (when just formed, it is virtually identical isotopically to the mantle at its origin) cannot be solved easily. Isotopic data are very helpful to distinguish old felsic crust from juvenile material, but cannot resolve juvenile material from the mantle or from mafic lower crust. This is particularly problematic for post-collisional settings, in which voluminous amounts of mantle melts have been accreted to the lower crust during the preceding subduction.

HKCA magmatism occurs typically in post-collisional setting, i.e., after a subduction and a collision period. It indicates that the K-enrichment of the source, which has to be recent to maintain juvenile isotope characteristics, most likely dates back to events during the preceding subduction period. If the juvenile source is considered to be young lower crust, then a remelting of high-K andesites formed during the subduction stage has to be envisaged (Roberts and Clemens, 1993). The problem of K-enrichment is then shifted to the generation of these high-K andesites by mantle melting. It is generally assumed that dehydration or melting of the subducting oceanic plate provokes a potassium metasomatism or hybridization of the overlying lithospheric mantle (e.g., Best, 1975), which partially keeps this signature through the crystallization of phlogopite and K-richrichterite (Wyllie and Sekine, 1982; Mitchell, 1995; Konzett et al., 1997) and become strongly inhomogeneous. Whatever the origin of these heterogeneities, this is an important point to allow the generation of potassic magmas (Foley, 1992a). The melting temperature of these minerals can be readily reached after the collision when the depression of the regional isotherms as a result of subduction vanishes. The particularly fertile and fusible pockets of volatile-enriched and K-rich mantle zones will preferably melt, giving rise to the HKCA series or even to shoshonitic series (Turner et al., 1996). The partial melting of these enriched mantle minerals explains the SNY parameter in the binary NYTS

diagram (Fig. 10). It provokes the preferential enrichment (relatively to the reference YT series) of the elements associated to K, Rb, Th and U. A Nb-Ta enrichment would be less expected in the case of dehydration of the subducted plate; but partial melts from the slab could enrich the mantle wedge in this element, as they modify also the ratios of Nb and Ta (Stolz et al., 1996), which may be trapped in the form of titanate minerals (Briqueu et al., 1984). These latter minerals can have also a non-subduction origin although often grouped with K-enriched mantle assemblage (Sheppard and Taylor, 1992). They are invoked as the cause of the Nb-Ta negative anomalies in non-subduction related potassic magmas due to their high stability under highly oxidising conditions (Foley and Wheller, 1990). If these K–Nb–Ta enriched mantle pockets are melted in response to rising of geotherms depressed by former subduction, no particular oxidized conditions have to be envisaged. This implies that these Nb–Ta enriched zones, probably associated with those enriched in K, could be also preferentially remobilized during the post-collisional period.

Active margin andesites are only the emerged part of the potassium enrichment provoked by the subduction process. The largest part of the K-enrichment is indeed trapped within the lithospheric mantle that constitutes a huge reservoir of readily available K-rich components during the post-collisional period. Shoshonites are the most enriched rocks within the calc-alkaline series as well as the hottest and the latest manifestations within the post-collisional period. This could be linked to lithospheric delamination and consequent rise of the asthenosphere as in Tibet (Turner et al., 1996), although not necessarily on such a large scale and with no asthenospheric melts (see below).

The alkaline enrichment as enhanced by the SNX parameter in the NYTS binary diagram (Fig. 10) corresponds to the classical enrichment in HFS elements in the ocean island basalts (Sun and McDonough, 1989). This could be linked to the appearance of a mantle plume, as is often proposed for this type of magmatism. However, we do not favour such an interpretation, because it had to occur in the right place at the right moment, as post-collisional alkaline magmatism is frequent but not erratic. We prefer to consider a generally widespread and ubiquitous pas-

sive OIB or alkaline-type enrichment of the lowest lithosphere (TBL; thermal boundary layer) and of the upper asthenosphere (Anderson, 1995; Black and Liégeois, 1993), leading to a veined lower lithosphere. This could be a difference with potassic magmas for which the source is more probably the upper lithosphere (MBL; mechanical boundary layer) also veined (Foley, 1992b). This alkaline source would be mobilized when deep lithospheric structures reach it. This will particularly occur when deep lithospheric faults will induce local lithospheric delamination, allowing the upper enriched asthenosphere to rise, shearing off parts of the hot and ductile lower lithosphere (Liégeois and Black, 1987; Black and Liégeois, 1993; Tack et al., 1994). The asthenospheric uprising could provoke an important, though local, decompression partial melting (Black et al., 1985; Bailey, 1993), which explains the short duration of this kind of magmatism. The delaminated mantle can be rapidly replaced by freezing mafic rocks, the necessary complements of the mainly silicic alkaline complexes observed near the surface. The similarity between alkaline granitoids generated within the post-collisional and anorogenic settings is explained by the identical source (lower lithosphere/asthenosphere) and slight movements along lithospheric mega-shear zones but with devastating consequences ('harpoon effect'; Black et al., 1985) in this near-melting temperature source. The alkaline vs. peralkaline composition can probably be attributed to later differentiation effects. For example, in the Tin Zebane dyke swarm (NW Tuareg shield), both the peralkaline and metaluminous alkaline series have the same prevalent mantle signature ($\epsilon_{\text{Nd}} = +6.2$ and $\text{Sr}_i = 0.7028$ at 600 Ma) implying an identical juvenile source, likely to be the mantle itself (Hadj Kaddour et al., 1998).

The similar geodynamical scenario proposed for post-collisional alkaline and shoshonitic groups (lithospheric delamination) is offset by distinctive sources: subduction-modified upper lithosphere for shoshonitic rocks and enriched lower lithosphere–asthenosphere for alkaline rocks. This can be related to the intensity of the delamination and/or to the lithospheric tectonics that allow more or less deep magmas to rise. The role of fluids is also important, in particular for alkaline rocks, but this is a factor probably related to the source itself.

The two trends observed within the stratoid granites of Madagascar (Nédélec et al., 1995; Fig. 10C) indicate that the two sources, i.e., the potassic lithospheric mantle and the alkaline lowest lithosphere and asthenosphere can generate magmas at the same time. The peculiar tectonic environment of these granites, which are emplaced as a thick sequence of sheets, confirms that they intruded at a hinge moment in the post-collisional period of this area.

9. Conclusions

This study is based on a large geochemical data-bank of post-collisional granitoids from the Tuareg shield. The dominant high-K calc-alkaline (HKCA) magmatism evolves either to large quantities of alkaline-peralkaline plutons and volcanism (Adrar des Iforas, Mali) or to minor amounts of shoshonitic rocks (Aïr, Niger). To compensate for inherent limitations of the conventional geochemical approach, a sliding normalization is introduced to compare different magmatic series. The normalization is done relatively to a magmatic series and not to a unique rock. Here, the Yenchichi 2-Telabit series (54–77% SiO₂) has been chosen for normalization after having been fitted to a second-order polynomial. NYTS (normalized to Yenchichi 2-Telabit series) spidergrams and SNX/SNY-derived diagrams led us to propose two different sources for the HKCA-shoshonitic series and for the alkaline-peralkaline series. Both sources are mainly juvenile as indicated by Sr and Nd isotopes.

HKCA magmatism typically occurs in large batholiths, such as is the case in the Tuareg shield (Black et al., 1994). This has been linked to large movements along mega-shear zones due to oblique subduction of small oceanic basins in a post-collisional setting (Liégeois et al., 1987, 1994). Major episodes of Mesozoic plutonism in California correlate also with periods of oblique subduction and trench parallel transport of western California along intrabatholithic faults (Glazner, 1991). The post-collisional period is defined here as the period that follows a major collision and concomitant high-pressure metamorphism. The main characteristics of the post-collisional period are the large movements of terranes along mega-shear zones and the rise of the regional isotherms, which were depressed by the

subduction of large oceanic plates. This implies that sources thermally stable during the active margin period can melt during the post-collisional period. The post-collisional setting shifts to an anorogenic intraplate setting when all these terranes are welded.

The source of HKCA-shoshonitic magmatism is enriched in K, Rb, Th, U and Ta relatively to the reference series of Yenchichi 2-Telabit and is mainly juvenile judging from Sr–Nd isotopic ratios. Contamination by old continental crust had only a slight influence on the magma composition. This source can correspond either to a juvenile crust composed of high-K andesites (Roberts and Clemens, 1993), which raises the problem of the origin of these andesites, or to phlogopite-K-richterite enriched lithospheric mantle. In both cases, the main point is that the generation of the HKCA magma needs the former existence of an important subduction phase to generate its source. Moreover, favourable conditions for melting of this source and for emplacement of large amount of granitoids have to exist. This implies an elevation of temperature to melt the most fusible parts of the lithospheric mantle and a favourable tectonic environment, in particular strike-slip faulting to allow the emplacement of batholiths (Glazner, 1991). This is probably the reason why HKCA magmatism is so abundant in the post-collisional period that meets these conditions, i.e., uprising of isotherms after subduction, displacement of terranes.

Observations show that alkaline granitoids can be generated in several environments (anorogenic, post-collisional, island arc, continents and oceans...) with similar geochemical characteristics. This indicates that the alkaline source is ubiquitous and widespread, favouring the base of the lithosphere and the upper asthenosphere (Black and Liégeois, 1993), where hybridisation of several geochemical 'reservoirs' can occur on a global scale. Lithospheric movements, even small, particularly in the reverse sense ('harpoon effect'; Black et al., 1985), can provoke partial melting of this hot source by decompression, which removes the problem of the origin of the extra-heat (Sylvester, 1989). Alkaline magmatism is linked to major lithospheric structures, whether it is post-collisional (Boullier et al., 1986; Liégeois and Black, 1987; Duchesne et al., 1997; Nardi and Bonin, 1991) or anorogenic (Black et al., 1985; Moreau et al., 1994; Fig. 2B).

The transition from HKCA to alkaline magmatism at the end of the orogeny is not a rare phenomenon (Bonin, 1990). Two different models can explain this transition. (1) When the regional isotherms, depressed during the main subduction event, are restored, only the deeper source of the alkaline series at the base of the lithosphere or in the upper asthenosphere can still melt. (2) A more rapid switch to melting conditions by rapid rise of hot asthenosphere material due to a slab break-off (Liégeois and Black, 1987; Davies and von Blanckenburg, 1995) or to lithospheric delamination (Black and Liégeois, 1993; Tack et al., 1994).

Geochemical characteristics point to the composition of the source of the granitoids and not to their geotectonic setting (Pearce et al., 1984; Sylvester, 1989). However, conditions of partial melting have to be met for the considered source to generate magmas. Some geotectonic settings will be more propitious to generate certain types of magmatism and some will be more 'specialized' than others. The post-collisional period appears to be particularly efficient to mobilize various kind of sources (Tack et al., 1994) mainly due to large movements along mega-shear zones, to the availability of modified, still hot sources generated by the preceding subduction period and to important and rapid modifications of the lithospheric structure and temperature, both at the crustal and mantle level. All these events result from the preceding collisional process, justifying the use of the expression 'post-collisional'.

Acknowledgements

We warmly thank Bernard Bonin, Daniel Demaiffe, Jean-Clair Duchesne and Louis Latouche for frequent discussions. Detailed and constructive reviews of Paul J. Sylvester and Jacques Leterrier have greatly contributed to the amelioration of this paper.

Appendix A. Analytical techniques

A.1. Major elements

308 samples have been analyzed. Si, Al, Ti, Fe, Ca and P have been analyzed by X-ray fluorescence

following the method described by Norrish and Hutton (1969); Mn, Mg, K and Na have been measured by atomic absorption spectrometry after open acid digestion ($\text{HF} + \text{HClO}_4 + \text{HNO}_3$); FeO has been determined by redox titration with permanganate solution.

A.2. Trace elements

X-ray fluorescence of ground powder material was used for Rb and Sr (308 samples). For the other trace elements (86 samples), two analytical techniques have been used: for 23 samples, a standard instrumental neutron activation (INAA) on pressed powder pellets was used, while the 63 other samples were analyzed by ICP-MS (VG PQ2 +). In the latter case, the result of the alkaline fusion (0.3 g of sample + 0.9 g of lithium metaborate at 1000°C during one hour) has been dissolved in 5% HNO_3 . The calibrations were set using both synthetic solution (mixture of the considered elements at 2, 5 and 10 ppb) and international rock standards (BHVO-1, W1, GA, ACE). For all these elements, the precision varies from 5 to 10% (for details, see Navez, 1995). Trace element analyses comprising Sc concentrations have been acquired by INAA, the others by ICP-MS.

References

- Anderson, D.L., 1995. Lithosphere, asthenosphere and perisphere. *Rev. Geophys.* 33, 125–149.
- Azzouni-Sekkal, A., Boissonnas, J., 1993. Une province magmatique de transition du calco-alkalin à l'alkalin: les granitoïdes pan-africains à structures annulaires de la chaîne pharusienne du Hoggar (Algérie). *Bull. Soc. Géol. Fr.* 164, 597–608.
- Ba, H., Black, R., Benziene, B., Diombana, D., Hascoet-Fender, J., Bonin, B., Fabre, J., Liégeois, J.P., 1985. La province des complexes annulaires alcalins sursaturés de l'Adrar des Iforas, Mali. *J. Afr. Earth Sci.* 3, 123–142.
- Bailey, D.K., 1993. Petrogenetic implications of the timing of alkaline, carbonatite, and kimberlite igneous activity in Africa. *S. Afr. J. Geol.* 96, 67–74.
- Bertrand, J.M., Dupuy, C., Dostal, J., Davison, I., 1984. Geochemistry and geotectonic interpretation of granitoids from Central Iforas (Mali W. Africa). *Precamb. Res.* 26, 265–283.
- Best, M.G., 1975. Migration of hydrous fluids in the upper mantle and potassium variation in calc-alkalic rocks. *Geology* 3, 429–432.
- Bigoggero, B., Colombo, A., Del Moro, A., Gregnanin, A., Macera, P., Tunesi, A., 1994. The Oligocene Velle del Cervo

- Pluton: an example of shoshonitic magmatism in the western Italian Alps. *Mem. Sci. Geol.* Padova 46, 409–421.
- Black, R., 1967. Carte géologique de reconnaissance du massif de l'Air à l'échelle de 1:500000. Ministère des Mines et de l'Énergie, République du Niger, Niamey.
- Black, R., Girod, M., 1970. Late Palaeozoic to Recent igneous activity in West Africa and its relationship to basement structure. In: Clifford, T.N., Gass, I.G. (Eds.), *African Magmatism and Tectonics*, Oliver and Boyd, Edinburgh, pp. 185–210.
- Black, R., Liégeois, J.-P., 1993. Cratons, mobile belts, alkaline rocks and continental lithospheric mantle: the Pan-African testimony. *J. Geol. Soc. London* 150, 89–98.
- Black, R., Caby, R., Moussine-Pouchkine, A., Bayar, R., Bertrand, J.M.L., Boullier, A.M., Fabre, J., Lesquer, A., 1979. Evidence for late Precambrian plate tectonics in West Africa. *Nature* 278, 223–227.
- Black, R., Lameyre, J., Bonin, B., 1985. The structural setting of alkaline complexes. *J. Afr. Earth Sci.* 3, 5–16.
- Black, R., Liégeois, J.P., Navez, J., Vialette, Y., 1991. Terrains exotiques dans les zones internes de la chaîne pan-africaine trans-saharienne: les clefs fournies par l'Air sud-oriental (République du Niger). *C. R. Acad. Sci. Paris* 312, 889–895.
- Black, R., Latouche, L., Liégeois, J.P., Caby, R., Bertrand, J.M., 1994. Pan-African displaced terranes in the Tuareg shield (central Sahara). *Geology* 22, 641–644.
- Bonin, B., 1986. Ring Complex Granites and Anorogenic Magmatism. *Studies in Geology*, North Oxford Academic, Oxford, and Elsevier, Amsterdam, 188 pp.
- Bonin, B., 1990. From orogenic to anorogenic settings: evolution of granitoid suites after a major orogenesis. *Geol. J., W.S. Pitcher Special Issue* 25, 261–270.
- Bonin, B., Lameyre, J., 1978. Réflexions sur la position et l'origine des complexes magmatiques anorogéniques. *Bull. Soc. Géol. Fr.* 20, 45–59.
- Bonin, B., Platevoet, B., Vialette, Y., 1987. The geodynamic significance of alkaline magmatism in the western Mediterranean compared with West Africa. In: Bowden, P., Kinnaird, J.A. (Eds.), *African Geology Reviews*, *Geol. J. Thematic Issue* 22, 361–387.
- Boullier, A.M., Liégeois, J.P., Black, R., Fabre, J., Sauvage, M., Bertrand, J.M., 1986. Late Pan-African tectonics marking the transition from subduction-related calc-alkaline magmatism to within-plate alkaline granitoids (Adrar des Iforas Mali). *Tectonophysics* 132, 233–246.
- Briqueu, L., Bougault, H., Joron, J.L., 1984. Quantification of Nb, Ta, Ti and V anomalies in magmas associated with subduction zones: petrogenetic implications. *Earth Planet. Sci. Lett.* 68, 297–308.
- Caby, R., Andreopoulos-Renaud, U., 1985. Etude pétrostructurale et géochronologique U/Pb sur zircon d'une métadiorite quartzique de la chaîne pan-africaine de l'Adrar des Iforas (Mali). *Bull. Soc. Géol. Fr.* 8, 899–903.
- Caby, R., Bertrand, J.M., Black, R., 1981. Pan-African closure and continental collision in the Hoggar-Iforas segment, Central Sahara. In: Kröner, A. (Ed.), *Precambrian Plate Tectonics*, Elsevier, Amsterdam, pp. 407–734.
- Caby, R., Andreopoulos-Renaud, U., Pin, C., 1989. Late Proterozoic arc-continent and continent-continent collision in the Pan-African Trans-Saharan belt of Mali. *Can. J. Earth Sci.* 26, 1136–1146.
- Clemens, J.D., Holloway, J.R., White, A.J.R., 1986. Origin of an A-type granite: experimental constraints. *Am. Mineral.* 71, 317–324.
- Davies, J.H., von Blanckenburg, F., 1995. Slab breakoff: a model of lithosphere detachment and its test in the magmatism and deformation of collisional orogens. *Earth Planet. Sci. Lett.* 129, 85–102.
- DeLong, S.E., Hodges, F.N., Arculus, R.J., 1975. Ultramafic and mafic inclusions, Kanaga island, Alaska, and the occurrence of alkaline rocks in island arcs. *J. Geol.* 83, 721–736.
- Duchesne, J.C., Wilmart, E., 1997. Igneous charnockites and related rocks from the Bjerkreim-Sokndal layered intrusion (Southwest Norway): a jotunite (hypersthene monzodiorite)-derived A-type granitoid suite. *J. Petrol.* 38, 337–369.
- Duchesne, J.C., Schärer, U., Liégeois, J.P., Vander Auwera, J., Longhi, J., 1997. Tectonic Setting and Phase Diagram Constraints on the Origin of Proterozoic Anorthositic: The Craton Tongue Melting Model. Abstract, Copena, Trondheim, Norway.
- Duchesne, J.C., Berza, T., Liégeois, J.P., Vander Auwera, J., 1998. Shoshonitic Liquid Line of Descent from Diorite to Granite: The Late Precambrian Post-collisional Tismana Pluton, South Carpathians, Romania. *Lithos* 45, 281–303.
- Fabre, J., 1982. Carte géologique et gravimétrique de l'Adrar des Iforas au 1:500000. Ministère de l'Énergie et des Mines, Direction Nationale de la Géologie et des Mines, République du Mali, Bamako.
- Foley, S., 1992a. Potassic and ultrapotassic magmas and their origin. *Lithos* 28, 181–186.
- Foley, S., 1992b. Vein-plus-wall-rock melting mechanisms in the lithosphere and the origin of potassic alkaline magmas. *Lithos* 28, 435–454.
- Foley, S., Wheller, G.E., 1990. Parallels in the origin of the geochemical signatures of island arc volcanics and continental potassic igneous rocks: the role of residual titanates. *Chem. Geol.* 85, 1–18.
- Glazner, A.F., 1991. Plutonism, oblique subduction, and continental growth: an example from the Mesozoic of California. *Geology* 19, 784–786.
- Hadj Kaddour, Z., Demaiffe, D., Liégeois, J.P., Caby, R., 1998. The Alkaline-peralkaline Granitic Post-collisional Tin Zebane Dyke Swarm, Pan-African Tuareg Shield, Algeria, Prevalent Mantle Signature and Late Agpaitic Differentiation. *Lithos* 45, 223–243.
- Janoušek, V., Rogers, G., Bowes, D.R., 1995. Sr–Nd isotopic constraints on the petrogenesis of the Central Bohemian pluton, Czech Republic. *Geol. Rundsch.* 84, 520–534.
- Konzett, J., Sweeney, R.J., Thompson, A.B., Ulmer, P., 1997. Potassium amphibole stability in the upper mantle: an experimental study in a peralkaline KNCMASH system to 8.5 GPa. *J. Petrol.* 38, 537–568.
- Le Maitre, R.W., 1989. *A Classification of Igneous Rocks and Glossary of Terms*. Blackwell Scientific Publications, Oxford, 193 pp.

- Liégeois, J.P., 1988. Le batholite composite de l'Adrar des Iforas (Mali). *Académie royale des Sciences d'Outre-Mer, Classe des Sciences Naturelles et Médicales, Bruxelles, nouvelle série*, 22, 231 pp.
- Liégeois, J.P., Black, R., 1984. Pétrographie et géochronologie Rb-Sr de la transition calco-alkaline - alcaline fini-panafricaine dans l'Adrar des Iforas (Mali): accréction crustale au Précambrien supérieur. In: Klerkx, J., Michot, J. (Eds.), *Géologie africaine—African Geology*, Tervuren, pp. 115–146.
- Liégeois, J.-P., Black, R., 1987. Alkaline magmatism subsequent to collision in the Pan-African belt of the Adrar des Iforas. In: Fitton, J.G., Upton, B.G.J. (Eds.), *Alkaline Igneous Rocks*. The Geological Society, Blackwell, Oxford, 30, 381–401.
- Liégeois, J.P., Bertrand, J.M., Black, R., 1987. The subduction- and collision-related Pan-African composite batholith of the Adrar des Iforas (Mali): a review. *Geol. J.* 22, 185–211.
- Liégeois, J.P., Black, R., Navez, J., Latouche, L., 1994. Early and late Pan-African orogenies in the Air assembly of terranes (Tuareg shield Niger). *Precamb. Res.* 67, 59–88.
- Liégeois, J.P., Berza, T., Tatu, M., Duchesne, J.C., 1996a. The Neoproterozoic Pan-African basement from the Alpine lower Danubian nappe system (South Carpathians Romania). *Precamb. Res.* 80, 281–301.
- Liégeois, J.P., Diombana, D., Black R., 1996b. The Tessalit ring complex (Adrar des Iforas, Malian Tuareg shield): a Pan-African, post-collisional, syn-shear, alkaline granite intrusion. In: Demaiffe, D. (Ed.), *Petrology and Geochemistry of Magmatic Suite of Rocks in the Continental and Oceanic Crusts, ULB-MRAC, Bruxelles*, pp. 227–244.
- Mitchell, R.H., 1995. Melting experiments on a sanidine phlogopite lamproïte at 4–7 Gpa and their bearing on the sources of lamproïtic magmas. *J. Petrol.* 36, 1455–1474.
- Moreau, C., Demaiffe, D., Bellion, Y., Boullier, A.M., 1994. A tectonic model for the location of Paleozoic ring-complexes in Air (Niger West Africa). *Tectonophys.* 234, 129–146.
- Nardi, L.V.S., Bonin, B., 1991. Post-orogenic and non-orogenic alkaline granite associations: the Saibro intrusive suite, southern Brazil—a case study. *Chem. Geol.* 92, 197–211.
- Navez, J., 1995. Détermination d'éléments en traces dans les roches silicatées par ICP-MS. *Rapport Annuel du Département de Géologie et Minéralogie 1993–1994 Musée Royal de l'Afrique Centrale, Tervuren, Belgique*, 139–147.
- Nédélec, A., Stephens, W.E., Fallick, A.E., 1995. The Panafrican stratoid granites of Madagascar: alkaline magmatism in a post-collisional extensional setting. *J. Petrol.* 36, 1367–1391.
- Norrish, K., Hutton, J.T., 1969. An accurate X-ray spectrographic method for the analysis of a wide range of geological samples. *Geochim. Cosmochim. Acta* 33, 431–453.
- Paquette, J.L., Caby, R., Djouadi, M.T., Bouchez, J.L., 1998. U-Pb dating of the end of the Pan-African orogeny in the Tuareg shield: the post-collisional syn-shear Tiouveine pluton (western Hoggar, Algeria) 45, 245–253.
- Peacock, M.A., 1931. Classification of igneous rocks. *J. Geol.* 39, 56–67.
- Pearce, J.A., 1996. Sources and settings of granitic rocks. *Episodes* 19, 120–125.
- Pearce, J.A., Harris, N.B.W., Tindle, A.G., 1984. Trace element discrimination diagrams for the tectonic interpretation of granitic rocks. *J. Petrol.* 25, 956–983.
- Peccerillo, R., Taylor, S.R., 1976. Geochemistry of Eocene calc-alkaline volcanic rocks from the Kastamonu area, northern Turkey. *Contrib. Mineral. Petrol.* 58, 63–81.
- Rickwood, P.C., 1989. Boundary lines within petrologic diagrams which use oxides of major and minor elements. *Lithos* 22, 247–264.
- Roberts, M.P., Clemens, J.D., 1993. Origin of high-potassium, calc-alkaline, I-type granitoids. *Geology* 21, 825–828.
- Sheppard, S., Taylor, W.R., 1992. Barium and LREE-rich, olivine-mica-lamprophyres with affinities to lamproïtes, Mt. Bunday, Northern Territory, Australia. *Lithos* 28, 303–325.
- Sørensen, H. (Ed.), 1974. *The Alkaline Rocks*. John Wiley, London, 622 pp.
- Stolz, A.J., Jochum, K.P., Spettel, B., Hofmann, A.W., 1996. Fluid- and melt-related enrichment in the subarc mantle: evidence from Nb/Ta variations in island-arc basalts. *Geology* 24, 587–590.
- Sylvester, P.J., 1989. Post-collisional alkaline granites. *J. Geol.* 97, 261–280.
- Sun, S.S., McDonough, W.F., 1989. Chemical and isotopic systematics of oceanic basalts: implications for mantle composition and processes. In: Saunders, A.D., Norry, M.J. (Eds.), *Magmatism in the Ocean Basins*. *Geol. Soc. Spec. Publ.* 42, 313–345.
- Tack, L., Liégeois, J.P., Deblond, A., Duchesne, J.C., 1994. Kibaran A-type granitoids and mafic rocks generated by two mantle sources in a late orogenic setting (Burundi). *Precamb. Res.* 68, 323–356.
- Turner, S., Arnaud, N., Liu, J., Rogers, N., Hawkesworth, C., Harris, N., Kelley, S., Van Calsteren, P., Deng, W., 1996. Post-collision, shoshonitic volcanism on the Tibetan plateau: implications for convective thinning of the lithosphere and the source of ocean island basalts. *J. Petrol.* 37, 45–71.
- Vail, J., 1989. Ring complexes and related rocks in Africa. *J. Afr. Earth Sci.* 8, 19–40.
- Vander Auwera, J., Horion, D., 1998. The Biella and Traversella Intrusions (Sesia-Lanzo zone, Italy): Examples of Two Post-collisional Shoshonitic and High-k Calc-alkaline Suites. 88th Annual Meeting, Geological Dynamics of Alpine Type Mountain Belts Ancient and Modern, Bern.
- Watson, E.B., Harrison, T.M., 1983. Zircon saturation revisited: temperature and compositional effects in a variety of crustal magma types. *Earth Planet. Sci. Lett.* 64, 295–304.
- Whalen, J.B., Currie, K.L., Chappell, B.W., 1987. A-type granites: geochemical characteristics, discrimination and petrogenesis. *Contrib. Mineral. Petrol.* 95, 407–419.
- Wyllie, P.J., Sekine, T., 1982. The formation of mantle phlogopite in subduction zone hybridization. *Contrib. Mineral. Petrol.* 79, 375–380.